Title

Linking leaf dark respiration to leaf traits and reflectance spectroscopy across diverse forest types

Authors

Wu, Fengqi
Liu, Shuwen
Lamour, Julien
et al.

Publication Date

2024-11-19

DOI

10.1111/nph.20267

Peer reviewed

New Phytologist

Linking leaf dark respiration to leaf traits and reflectance spectroscopy across diverse forest types

Journal:	*New Phytologist*
Manuscript ID	NPH-MS-2024-47948.R1
Manuscript Type:	Full Paper
Date Submitted by the Author:	16-Oct-2024
Complete List of Authors:	Wu, Fengqi; Chinese Academy of Sciences, Institute of Botany Liu, Shuwen; The University of Hong Kong, School of Biological Sciences Lamour , Julien ; Université de Toulouse, Centre de Recherche sur la Biodiversité et l'Environnement (CRBE) Atkin, Owen; Australian National University, ARC Centre of Excellence in Plant Energy Biology, Research School of Biology Yang, Nan; Institute of Botany Chinese Academy of Sciences, State Key Laboratory of Vegetation and Environmental Change Dong, Tingting; Institute of Botany Chinese Academy of Sciences, State Key Laboratory of Vegetation and Environmental Change Xu, Weiying; Institute of Botany Chinese Academy of Sciences, State Key Laboratory of Vegetation and Environmental Change Smith, Nicholas; Texas Tech University, Department of Biological Sciences Wang, Zhihui; Guangdong Academy of Sciences, Guangzhou Institute of Geography Wang, Han; Tsinghua University, Department of Earth System Science Su, Yanjun; Institute of Botany Chinese Academy of Sciences, State Key Laboratory of Vegetation and Environmental Change Liu, Xiaojuan; Institute of Botany Chinese Academy of Sciences, State Key Laboratory of Vegetation and Environmental Change Shi, Yue; Institute of Botany Chinese Academy of Sciences, State Key Laboratory of Vegetation and Environmental Change Xing, Aijun; Institute of Botany Chinese Academy of Sciences, State Key Laboratory of Vegetation and Environmental Change Dai, Guanhua; Chinese Academy of Sciences, Research Station of Changbai Mountain Forest Ecosystems Dong, Jinglong; Xishuangbanna Tropical Botanical Garden CAS Key Laboratory of Tropical Forest Ecology, CAS Key Laboratory of Tropical Forest Ecology, Xishuangbanna Tropical Botanical Garden, Chinese Academy of Sciences, Menglun, Mengla, Yunnan 666303, China Swenson, Nathan; University of Notre Dame, Bilogical Sciences Kattge, Jens; Max Planck Institute for Biogeochemistry, Biogeochemistry; German Centre for Integrative Biodiversity Research (iDiv) Halle-Jena-Leipzig, iDiv - German Centre for Integrative Biodiversity Research Halle-Jena-Leipzig Reich, Peter B. ; Western Sydney University, Hawkesbury Institute for the

	Environment; University of Minnesota, Department of Forest Resources; University of Michigan, Institute for Global Change Biology, and School for the Environment and Sustainability Serbin, Shawn; NASA Goddard Space Flight Center, Biospheric Sciences Laboratory, Code 618 Rogers, Alistair; Lawrence Berkeley National Laboratory, Climate & Ecosystem Sciences Division Wu, Jin; The University of Hong Kong, School for Biological Sciences Yan, Zhengbing; Institute of Botany Chinese Academy of Sciences, State Key Laboratory of Vegetation and Environmental Change
Key Words:	carbon cycling, gas exchange, leaf mitochondrial respiration, leaf spectroscopy, partial least-squares regression, plant functional traits, transferability
Suggested Handling Editor:	Richard Norby

Data Availability Statement

Our Mandates Data Policy requires data to be shared and a Data Availability Statement, so please enter one in the space below. Sample statements can be found here. Please note that this statement will be published alongside your manuscript, if it is accepted for publication.

The data supporting the results of the manuscript can be accessed via the Plant Science Data Center, Chinese Academy of Sciences using the following link: XXX (we will add it upon article acceptance)

Title: Linking leaf dark respiration to leaf traits and reflectance spectroscopy across diverse forest types

Author List: Fengqi Wu[1,2,3], Shuwen Liu[4], Julien Lamour[5], Owen K. Atkin[6], Nan Yang[1,2], Tingting Dong[1,2,3], Weiying Xu[1,2,3], Nicholas G. Smith[7], Zhihui Wang[8], Han Wang[9], Yanjun Su[1,2,3], Xiaojuan Liu[1,2,3], Yue Shi[1,2], Aijun Xing[1,2], Guanhua Dai[10], Jinlong Dong[3,11,12], Nathan G. Swenson[13], Jens Kattge[14,15], Peter B. Reich[16,17,18], Shawn P. Serbin[19], Alistair Rogers[20], Jin Wu[4], Zhengbing Yan[1,2,3*]

Author Affiliations:

(1) State Key Laboratory of Vegetation and Environmental Change, Institute of Botany, Chinese Academy of Sciences, Xiangshan, Beijing 100093, China.

(2) China National Botanical Garden, Beijing 100093, China.

(3) University of Chinese Academy of Sciences, Yuquanlu, Beijing 100049, China.

(4) Division for Ecology and Biodiversity, School of Biological Sciences, The University of Hong Kong, Hong Kong, China.

(5) Centre de Recherche sur la Biodiversité et l'Environnement (CRBE), Université de Toulouse, CNRS, IRD, Toulouse INP, Université Toulouse 3 – Paul Sabatier (UT3), Toulouse, France.

(6) Division of Plant Sciences, Research School of Biology, Australian National University, Canberra, 2601, ACT, Australia.

(7) Department of Biological Sciences, Texas Tech University, Lubbock, Texas USA 79409.

(8) Guangdong Provincial Key Laboratory of Remote Sensing and Geographical Information System, Guangdong Open Laboratory of Geospatial Information Technology and Application, Guangzhou Institute of Geography, Guangdong Academy of Sciences, Guangzhou, China.

(9) Department of Earth System Science, Ministry of Education Key Laboratory for Earth System Modeling, Institute for Global Change Studies, Tsinghua University, Beijing 100084, China.

(10) Research Station of Changbai Mountain Forest Ecosystems, Chinese Academy of Sciences, Antu 133613, China.
(11) CAS Key Laboratory of Tropical Forest Ecology, Xishuangbanna Tropical Botanical Garden, Chinese Academy of Sciences, Mengla, Menglun 666303, China.
(12) National Forest Ecosystem Research Station at Xishuangbanna, Xishuangbanna Tropical Botanical Garden, Chinese Academy of Sciences, Mengla, Menglun 666303, Yunnan, China.
(13) Department of Biological Sciences, University of Notre Dame, Notre Dame, Indiana 46556, USA.
(14) Max Planck Institute for Biogeochemistry, Hans Knöll Str. 10, 07745 Jena, Germany.
(15) iDiv - German Centre for Integrative Biodiversity Research Halle-Jena-Leipzig, Puschstraße 4 04103 Leipzig, Germany.
(16) Hawkesbury Institute for the Environment, Western Sydney University, Locked Bag 1797, Penrith 2751, Australia.
(17) Department of Forest Resources, University of Minnesota, St. Paul, MN 55108, USA.
(18) Institute for Global Change Biology, and School for the Environment and Sustainability, University of Michigan, Ann Arbor, MI 48109, USA.
(19) Biospheric Sciences Laboratory, NASA Goddard Space Flight Center, Greenbelt, MD, 20771.
(20) Climate & Ecosystem Sciences Division, Lawrence Berkeley National Laboratory, Berkeley, CA 94720 USA.

* Corresponding Author: Zhengbing Yan
State Key Laboratory of Vegetation and Environmental Change, Institute of Botany, Chinese Academy of Sciences, Xiangshan, Beijing 100093, China (E-mail: zbyan@ibcas.ac.cn; phone: +010 - 6283 6252)

Figures/Tables/Words Record:
Number of figures/tables: 8 figures, 1 table

57 Supporting information: 9 figures, 3 tables, 3 methods

58

59 **Words count:** Summary: 199; Introduction: 1408; Materials and Methods: 1874; Results: 833;

60 Discussion: 2714; Total word count (excluding summary, references, and legends): 6828.

Summary

- Leaf dark respiration (R_{dark}), an important yet rarely quantified component of carbon cycling in forest ecosystems, is often simulated from leaf traits such as the maximum carboxylation capacity (V_{cmax}), leaf mass per area (LMA), nitrogen and phosphorus concentrations, in Terrestrial Biosphere Models. However, the validity of these relationships across forest types remains to be thoroughly assessed.
- Here we analyzed R_{dark} variability and its associations with V_{cmax} and other leaf traits across three temperate, subtropical and tropical forests in China, evaluating the effectiveness of leaf spectroscopy as a superior monitoring alternative.
- We found that leaf magnesium and calcium concentrations were more significant in explaining cross-site R_{dark} than commonly-used traits like LMA, nitrogen and phosphorus concentrations, but univariate trait-R_{dark} relationships were always weak ($r^2 \leq 0.15$) and forest-specific. Although multivariate relationships of leaf traits improved the model performance, leaf spectroscopy outperformed trait-R_{dark} relationships, accurately predicted cross-site R_{dark} ($r^2=0.65$), and pinpointed the factors contributing to R_{dark} variability.
- Our findings reveal a few novel traits with greater cross-site scalability regarding R_{dark}, challenge the use of empirical trait-R_{dark} relationships in process models, and emphasize the potential of leaf spectroscopy as a promising alternative for estimating R_{dark}, which could ultimately improve process modeling of terrestrial plant respiration.

Key words: carbon cycling, gas exchange, leaf mitochondrial respiration, leaf spectroscopy, partial least-squares regression, plant functional traits, transferability

Introduction

Land plant respiration, a major component of the global carbon (C) cycling and vegetation-climate interactions (Wang *et al.*, 2020a), releases ca. 60 Pg C/year to the atmosphere, that is six times higher than human-induced CO_2 emissions (Ciais *et al.*, 2014). About half of C released by plant respiration is derived from leaf dark respiration (R_{dark} – i.e., non-photorespiratory mitochondrial CO_2 release) that takes place during the day and night (Atkin *et al.*, 2007; Huntingford *et al.*, 2017), with the release of CO_2 being coupled to production of energy in the form of adenosine-triphosphate (ATP) and reducing equivalents. Leaf R_{dark} plays an important role in nitrogen (N) assimilation, C skeleton synthesis and the regulation of redox balance (Atkin *et al.*, 2015; Garcia *et al.*, 2022).Because of the strong kinetic response of R_{dark} to temperature, R_{dark} is typically converted to a rate at a standardized temperature, such as 25°C (R_{dark25}), reflecting respiratory capacity (Atkin and Tjoelker, 2003; Atkin *et al.*, 2007; Davidson *et al.*, 2023b). As a result, R_{dark25} has long been identified as a crucial biochemical parameter in Terrestrial Biosphere Models (TBMs) (Huntingford *et al.*, 2017), and accurate representation of R_{dark25} in TBMs greatly influences the precision of simulations of terrestrial plant productivity and carbon cycling (Schwalm *et al.*, 2010; Atkin *et al.*, 2015; Butler *et al.*, 2021). However, R_{dark25} is highly variable, in response to differences in energy demand among contrasting plant species, plant functional groups, ecosystem types, climate, soil conditions, and acclimation (Lambers and Oliveira, 2008; Atkin, 2011; Atkin *et al.*, 2015; Reich *et al.*, 2016). Therefore, efficient and accurate characterization of leaf R_{dark25} across ecosystems – particularly among different forest types – will be crucial if we are to improve representation of plant respiration in TBMs. The ability to rapidly quantify variation in R_{dark25} is also essential if we are to develop a more thorough mechanistic understanding of the factors that drive R_{dark25} in nature.

R_{dark25} is closely intertwined to photosynthetic metabolism through reliance of respiration on substrates from photosynthesis and demands for respiratory products (e.g., ATP) to support maintenance and export processes that are closely linked to photosynthesis (Fan *et al.*, 2021;

Fernie *et al.*, 2004). Because Ribulose-1,5-bisphosphate carboxylase/oxygenase (Rubisco) is the largest and most energy demanding enzyme in the photosynthetic process, TBMs commonly assume R_{dark25} to be proportional to the maximum carboxylation capacity of the enzyme Rubisco standardized to a reference temperature of 25°C (V_{cmax25}) in TBMs (Schwalm *et al.* 2010; Atkin *et al.*, 2015). An example is how R_{dark25} and V_{cmax25} are set by a commonly assumed coefficient (R_{dark25}:V_{cmax25} ratio=0.015) in several TBMs (Clark *et al.*, 2011; Atkin et al. 2017; Fan *et al.*, 2021). Alternatively, R_{dark25} can be extrapolated using its empirical relationships with other relatively easy-to-measure leaf traits, such as leaf-mass-per-area (LMA), leaf N and phosphorus (P) concentrations, which have more extensive spatial coverage (Reich *et al.*, 1998b; Atkin *et al.*, 2015; Rowland *et al.*, 2016; Ren *et al.*, 2023). However, the relationships between R_{dark25} and leaf traits vary in nature, influenced by multiple biotic and abiotic variables (Wright *et al.*, 2006; Reich *et al.*, 2008; Atkin *et al.*, 2015; O'Leary *et al.*, 2017), leading to uncertainties that restrict the fine-scale R_{dark25} explanations and predictions within and across forest biomes.

Besides the widely studied leaf economics traits (i.e., V_{cmax25}, LMA, leaf N and P concentrations) that are related to R_{dark25}, other leaf elements might also crucially explain R_{dark25} variability (Atkin *et al.*, 2011; O'Leary *et al.*, 2017; Tcherkez *et al.*, 2024). Magnesium (Mg), a core component of the energy transfer process in leaf respiratory metabolism, plays a crucial role in ATP synthesis and hydrolysis through the Mg-ATP/ADP complex, which can bind up to 50% of the total cellular Mg concentration (Maguire and Cowan, 2002; Cakmak and Yazici, 2010; Chen *et al*., 2018). Manganese (Mn) shares similar ionic radii with Mg, and the two elements can substitute for each other in metal-binding sites, resulting in co-regulation of respiration rates in plants (Bloom & Kameritsch, 2017). Calcium (Ca) can affect leaf respiration processes as it acts as both the signal transduction ion that binds to a variety of respiratory-related carriers (e.g. mitochondrial aspartate/glutamate carrier and ATP-Mg/Pi carrier) (Bhosale *et al.*, 2015; Rueda *et al.*, 2016), and the activator of mitochondrial dehydrogenase (Satrústegui *et al.*, 2007). Potassium (K) can differentially regulate the

activities of glycolysis and tricarboxylic acid cycle (TCA) involved in mitochondrial respiration processes (Okamoto, 1967, 1968; Cui *et al.*, 2019). Sulphur (S) in thioredoxin participates in the redox regulation that largely affects plant respiratory function, by binding to respiratory proteins (Balmer *et al.*, 2004; Gelhaye *et al.*, 2004). Despite their importance for respiratory metabolism, little attention has been paid to how variation in R_{dark25} is linked to differences in Mg, Mn, Ca, K and/or S abundance in leaves across terrestrial forest ecosystems.

Additionally, large-scale surveys of R_{dark25} variability and mechanistic understanding of its driving factors are also greatly limited by traditional R_{dark25} measurement (Garcia *et al.*, 2022), determined by measuring the changing flux rate of oxygen or carbon dioxide concentrations in dark-adapted leaves (Long and Bernacchi, 2003; Coast *et al.*, 2019; Lamour *et al.*, 2021), which is often time-consuming and labor-intensive, and may be limited by canopy access. Therefore, an efficient, rapid and accurate alternative for characterization of R_{dark25} variability remains particularly imperative. Leaf reflectance spectroscopy has shown a substantial potential in multi-scale monitoring of leaf trait variations within and across terrestrial ecosystems (Asner *et al*., 2016; Fu *et al.*, 2020; Serbin & Townsend, 2020; Lamour *et al.*, 2023; Liu *et al.*, 2024). This potential arises primarily from the strong connection between the emergent continuous leaf reflectance spectrum with respect to solar radiation and a broad suite of underlying leaf structural, biochemical, and nutritional characteristics that drive the reflectance signatures through the interaction of radiation within internal leaf electronic and vibrational absorption properties (Curran, 1989; Elvidge, 1990; Kokaly *et al*., 2009). By employing statistical modeling methods such as partial least squares regression (PLSR) that harness the full-band leaf reflectance spectra, key signal bands related to target traits can be identified (Ollinger and Smith, 2005; Serbin *et al*., 2014) and the primary mechanisms underlying spectral predictions can be verified (Chavana-Bryant *et al*., 2016; Dechant *et al*., 2017; Meacham-Hensold *et al*., 2019). Accordingly, a multitude of studies has confirmed that leaf reflectance spectroscopy can estimate a wide range of leaf morphological, biochemical to physiological traits. Leaf spectroscopy should also be efficient to estimate R_{dark25}, as it can effectively predict LMA and

168 V_{cmax25} and empirically estimate leaf nutrient (N, P, K, Ca, Mg, S and Mn) concentrations, all
169 of which are loosely associated with R_{dark25} (Serbin *et al*., 2019; Asner *et al*., 2016; Yan *et al*.,
170 2021; Kothari *et al.*, 2023). Recent studies have indeed revealed the potential capacity of leaf
171 spectroscopy to predict variation in R_{dark25} in wheat (Coast *et al.*, 2019) and in a tropical forest
172 ecosystem (Lamour *et al.*, 2021). Therefore, we suspect that spectroscopy is likely to be a
173 promising alternative approach for characterizing how R_{dark25} varies across a large breadth of
174 trait and spectra space and across several terrestrial ecosystems. However, the prior studies of
175 spectra-R_{dark25} models are constrained to a limited number of species and forest types, and the
176 generalizability of spectra-R_{dark25} models remains unknown across diverse forest ecosystems.
177
178 The goal of this study was to explore linkages between R_{dark25} and leaf traits both within and
179 across diverse forest types, and evaluate the performance of leaf reflectance spectroscopy as a
180 more efficient alternative for predicting R_{dark25}. Specifically, we addressed the following two
181 questions:
182 (1) How do the empirical relationships of R_{dark25} with V_{cmax25} and with leaf morphological
183 and biochemical traits vary within and across forest types?
184 (2) Can leaf reflectance spectroscopy provide an efficient and robust alternative for
185 predicting R_{dark25} within and across forest types?
186 To address these questions, we collected a dataset of R_{dark25}, V_{cmax25}, LMA, leaf N, P, K, Ca,
187 Mg, S and Mn concentrations, and leaf reflectance spectra of canopy trees from three different
188 forest sites. These sites are located across a large latitudinal gradient, and include a temperate,
189 mixed needle-/broad-leaved forest, a subtropical evergreen broad-leaved forest, and a tropical
190 evergreen broad-leaved forest, hence achieving a broader comparison of species and forest
191 types than incorporated in previous studies. Through addressing these questions, we hope this
192 work can foster the mechanistic understanding and effective monitoring of R_{dark25} variability
193 across forest types, and improve the representation of leaf R_{dark25} in TBMs to better model
194 terrestrial plant respiration and the C cycle.
195

Materials and Methods

Study sites and plant materials

This study was conducted at three forest sites in China (Fig. 1): (1) Mountain Changbai (CB; 42°24'N, 128°06'E), a temperate, mixed needle- broad-leaved forest with a mean annual temperature (MAT) of 2.8°C and a mean annual precipitation (MAP) of 691 mm (He *et al.*, 2019); (2) Mountain Gutian (GT; 29°15'N, 118°07'E), a subtropical evergreen broad-leaved forest with a MAT of 15.3°C and a MAP of 1963.7 mm (Ning *et al.*, 2013); and (3) Xishuangbanna (XSBN; 21°47'N, 101°03'E), a tropical evergreen broad-leaved forest with a MAT of 21.8°C and a MAP of 1493 mm (Shen *et al.*, 2018). The three sites are representative of the range of forests found in China, and span a great diversity of biotic (tree species and forest types) and abiotic (temperature, precipitation, and soil properties) conditions (detailed information on soil pH, organic carbon, total nitrogen and total phosphorus are provided in Table S1). This large range in species and abiotic environmental conditions create the opportunity to investigate trait and spectral variation and evaluate more generalizable approaches (Guo *et al.*, 2022).

In the three forest sites, Chinese Academy of Sciences operates a tower crane that we used/accessed to collect sunlit leaves from the representative canopy trees. The tower crane facilities enabled access to a 1-hectare area of each forest site, and the crane tower was 40 m high at CB, 60 m at GT and 81 m at XSBN. Specifically, 80 trees from 9 dominant canopy tree species in CB (Liu *et al.*, 2023; Yan *et al.*, 2021), 93 trees from 17 dominant canopy tree species in GT (Hu *et al.*, 2005), and 95 trees from 39 dominant canopy tree species in XSBN (Liu *et al.*, 2023; Shen *et al.*, 2018) were selected as shown in Table S2. Sunlit branches in the upper canopy of these trees were sampled during the peak growing season (July-August) of 2023. We excised branches from the trees before dawn. The excised branches were immediately put in water and re-cut 10 cm away from the initial cut, ensuring that the branches always immersed during the sampling and measurements. These precautions were taken to avoid xylem embolisms and water stress (Wu *et al.*, 2016) and limit the impact of excision on leaf

physiology (Verryckt *et al.*, 2020; Akalusi *et al.*, 2021; Ferguson *et al*., 2023) and spectral reflectance (Haynes et al., 2024; also see Fig. S1). On each branch, we selected mature leaves to measure leaf gas exchange, leaf reflectance spectra, and leaf morphological and biochemical traits (i.e., LMA and leaf N, P, K, Ca, Mg, Mn, and S concentrations). The statistical results of these measurements are summarized in Table S2. The detailed protocols of measurement are described as follows.

Field measurements

Leaf gas exchange

Branch samples were stored in individual buckets and placed in the shade until used for leaf gas exchange measurements. We used six portable Li-COR gas exchange systems (two LI-6400XTs and four LI-6800s; Li-COR Inc., Lincoln, Nebraska, USA) simultaneously to measure the response of net assimilation rate (A) to intercellular carbon dioxide concentration (C_i) (commonly known as an A-C_i curve) and instantaneous leaf respiration in dark-adapted leaves (R_{dark}) between 6:00 and 17:00 each day. Our previous study has demonstrated that the type of Li-COR gas exchange system did not affect the results (Liu *et al.*, 2023).

Measurement of A-C_i curves closely followed Rogers *et al.* (2017) and Yan *et al.* (2021) with details shown in Method S1. Measurements of R_{dark} followed established protocols (Lamour *et al.*, 2021; Rowland *et al.*, 2016). The leaf was dark-adapted to eliminate the influence of light on leaf respiration (Shapiro *et al.*, 2004) for a period of 25 minutes, with the light source off and a dark cloth positioned on the instrument to avoid diffusion of light inside the chamber. The chamber conditions were set as follows: reference CO_2 concentration at 400 ppm, exchanger temperature set at the outside temperature to prevent the risk of condensation in the instrument, and flow rate at 350 μmol s^{-1} to maximize the signal to noise ratio. After the dark adaptation period, CO_2 exchange rates and chamber conditions were checked for stability over a 5-minutes' window before measurements occurred. Once stable, gas exchange was measured every 5 seconds for one minute to constitute one measurement of R_{dark}. To enable temperature-

standardized comparisons of respiration rate, we cross-compared two approaches to adjust R_{dark} to a reference temperature of 25°C (R_{dark25}). One method used an inverse Arrhenius equation (Davidson *et al.*, 2023b), while the other method used a temperature-dependent Q_{10} (Tjoelker *et al*., 2001) based on a known rate at measured temperature (as used in Atkin *et al.*, 2015). We found that R_{dark25} calculated by these two approaches was almost identical (Fig. S2), therefore chose the widely used method described by Davidson *et al.* (2023b) to calculate R_{dark25} (Bernacchi *et al.*, 2001, 2013; Von Caemmerer, 2013).

Leaf reflectance spectra

After completing the gas exchange measurements, we promptly measured the leaf reflectance spectra. A portable handheld contact-type spectrometer QualitySpec Trek (PANalytical, Boulder, Colorado, USA; spectral full-range: 400-2500 nm; spectral resolution: ≤3 nm at 700 nm, ≤9.8 nm at 1500 nm, ≤8.1 nm at 2100 nm; sampling internal: 1 nm through the linear interpolation) with a leaf clip was used to measure the spectral reflectance of leaves. At instrument startup, a 99% reflective Spectralon white reference disk (Labsphere Inc., North Dutton, NH, USA) was placed on the outside of the sampling window to calibrate the reflectance. The instrument was also calibrated automatically every half hour during operation using an internal white reference on the inside of the sampling window. Leaf spectral reflectance was calculated following the protocol by Wu *et al.* (2019) and Yan *et al.* (2021). Depending on leaf size, measurements were taken at 3 to 6 different positions on the adaxial side of each leaf, and the average reflectance for each wavelength was calculated as the reflectance spectrum of the leaf. During the collection of spectral data, issues such as spectral response saturation, instrument overheating, and abnormal spectral responses were addressed promptly according to prompts from the Trek instrument and the user manual.

Leaf biochemical and morphological traits

Following spectral measurements, the leaves without petiole were sampled for eight morphological and biochemical traits, including LMA, leaf N, P, K, Ca, Mg, Mn and S

concentrations. The measurements were performed via protocol in Method S2, and they provided mass-based estimates of elemental concentrations. To make it comparable with the area-based R_{dark25}, we convert them to area-based units for subsequent analysis.

Data analysis

Exploring trait-R_{dark25} relationships within and across forest types

To investigate the relationships between R_{dark25} and other leaf traits within and across the three forest sites, we conducted four analyses. Firstly, to examine the differences in leaf traits across forest types, we employed one-way analysis of variance (ANOVA) with the least significant difference (LSD) post-hoc test for multiple comparisons. To assess the individual contribution of each trait to the prediction of R_{dark25} within and across forest types, we performed ordinary least squares (OLS) regression and slope tests via R (v.4.3.2, R Core Team, 2013) package *smatr* on the relationships between R_{dark25} and other leaf traits. To rank the relative importance (RI) of each of the eight relatively easy-to-measure traits (i.e. LMA, leaf N, P, K, Ca, Mg, Mn, and S concentrations) in predicting R_{dark25}, the R package *relaimpo* (Wang *et al.*, 2021) was used to analyze based on data from all three forest sites. We explored the collective contribution of the eight relatively easier-to-measure traits to predicting R_{dark25} through multivariate linear regression. Specifically, we employed a multiple linear regressions as: lm (R_{dark25} ~ *trait variables*) to evaluate the predictive capability of these traits for R_{dark25} within and across the forest sites. A backward stepwise regression based on the Akaike Information Criterion (AIC) was used to determine whether traits with low relative importance could be excluded from the model. To ensure the validity and comparability, we implemented a repeated double cross-validation (rdCV) (Filzmoser *et al.*, 2009; see the subsequent section on PLSR modeling) consisting of 10-fold cross-validation with 200 repetitions. This method maintains consistency with the validation strategy employed in spectroscopy modeling (Fig. S3).

Developing spectral models of R_{dark25} and leaf morphological and biochemical traits

To establish the spectra-trait models, we followed existing protocols (Dechant *et al.*, 2017; Yan *et al.*, 2021; Burnett *et al.*, 2021). We adopted the PLSR method (Wold *et al.*, 2001) in conjunction with a rdCV, implemented using the Python library *scikit-learn* (Pedregosa *et al.*, 2011), to develop the spectra-trait models. The PLSR method, similar to principal component analysis (PCA), reduces the number of predictor variables down to a set of orthogonal latent variables (Liu *et al.*, 2023), and accommodates scenarios where the number of predictor variables greatly exceeds the number of response variables (Yan *et al.*, 2021). This enables PLSR to summarize complex spectral data, solve the problem of collinearity of variables, and achieve direct interpretation with linear regression, capturing the relationship between reflectance and physiological traits (Burnett *et al.*, 2021). Given these advantages, PLSR has been extensively applied in spectroscopic and chemometric analyses (Ollinger & Smith, 2005; Serbin *et al.*, 2014, 2019). The rdCV method separates the data repeatedly and randomly through cross-validation procedures into a calibration subset (containing training and test components) and an independent validation subset, and evaluates models were conducted on independent validation subsets generated from numerous possible random splits. This method thereby possesses the advantage of decreasing the odds of good or bad outcomes solely due to chance (Wu *et al.*, 2019). The modeling procedures have been shown by Dechant *et al.* (2017), Yan *et al.* (2021), and Liu *et al.* (2023b), and further modeling details are shown in Method S3, Figs. S3, S4 and S5.

Exploring the generalizability of spectra-R_{dark25} relationships under different spectral modeling scenarios

To test the generalizability of spectra-R_{dark25} model, we cross-compared PLSR model performance under two modeling scenarios: 'site-specific' and 'cross-site' scenario, and summarized the model performances in Table 1. In the 'site-specific' scenario, the spectra-R_{dark25} model was developed and evaluated using the data from each single forest site only. Each resulting PLSR model was then applied to the left-out data from the two other sites. With the 'cross-site' scenario, one spectra-R_{dark25} model was developed and evaluated using full

dataset from the three sites. These modeling tests allowed us to assess the generalizability of spectra-R_{dark25} relationships, and reveal potential scenarios and reasons for the deterioration of spectra-R_{dark25} relationships.

Cross-comparison of field-measured and spectra-modelled R_{dark25} variability in relation to leaf traits

To evaluate the influence of spectral model performance on trait-R_{dark25} relationships and the drivers of R_{dark25} variability, we explored the relationships between R_{dark25} and values of the other eight leaf morphological and biochemical traits predicted by the 'cross-site' spectral models. We then cross-compared these relationships with those derived from field measurements. Furthermore, we analyzed the inter- and intra-specific variation of leaf traits within each forest site, as well as in predicted values and direct field measurements across all sites following the method proposed by Guillén-Escribà *et al.* (2021). We used an ANOVA-based general linear model: $R_{dark25} \sim trait + species$, and partitioned the total variance among individual leaves by using the percentage of variance explained by the species term to represent the interspecific components, with the residuals representing the intraspecific components.

Results

Trait-R_{dark25} relationships and the relative importance of leaf traits for predicting R_{dark25} across forest types

To investigate our first question regarding trait-based methods for R_{dark25} predictions, we first analyzed the variations in R_{dark25}, V_{cmax25}-R_{dark25} relationships, and leaf morphological and biochemical traits within and across different forest types. We observed similar R_{dark25} in tropical and subtropical forest, but significant higher R_{dark25} in temperate forest compared to the other two forest types (p<0.001) (Fig. 2a). Subsequently, we found that R_{dark25}:V_{cmax25} ratio was 0.023 across the three forest sites and exhibited significant differences in these sites (p<0.001; Fig. 2b), with higher R_{dark25}:V_{cmax25} ratio at tropical forest in Xishuangbanna (0.026), followed by subtropical forest in GT (0.024), and temperate forest in CB (0.019). In addition, we found

that LMA and multi-elemental (except Mg) concentrations showed large variability within and across the three forest sites, with Ca concentration exhibiting the similar trends as R_{dark25} (Fig. S6). In addition, there were covariations among biochemical traits (Fig. S7).

To further explore the ability of traits to predict R_{dark25} at our sites, we conducted both univariate and multiple linear regressions (multiple traits have no collinearity effect on R_{dark25} (VIF<5)) (Figs. 3,4 & Table S3). We found that univariate trait-R_{dark25} relationships were weak ($r^2 \leq 0.13$), and that the slope and intercept of the linear regression was site dependent (Fig. 3). Both the univariate and multivariate analyses suggested that the best predictor of R_{dark25} variation was leaf Mg concentration (r^2=0.13, P<0.001; RI=23%), followed by leaf Ca (r^2=0.13, P<0.001; RI=21%), N (r^2=0.06, P<0.001; RI=17%), Mn (r^2=0.06, P<0.001; RI=15%), S (r^2=0.06, P<0.001; RI=10%), and P (r^2=0.06, P<0.001; RI=8%) concentrations (Fig. 3b-c,e-h&4b). Leaf K concentration (r^2=0.02, P<0.001; RI=4%) and LMA (r^2=0.00, P>0.05; RI=2%) were relatively poor predictors of R_{dark25} across forest types (Fig. 3a&d). Leaf K was removed from stepwise regression with AIC=22.20. Multiple linear regression models exhibited better R_{dark25} prediction (r^2=0.30; RMSE=0.25 μmol CO_2 m^{-2} s^{-1}) than univariate linear models across forest types (Figs. 3a-h&4b). In opposite to other nutrients, leaf Mn concentration showed a significantly negative relationship with R_{dark25} across diverse forest types (Fig. 3g).

Leaf reflectance spectroscopy outperforms leaf trait relationships in predicting R_{dark25} across forest types

We next examined the question of whether leaf reflectance spectra are sufficient to estimate R_{dark25} and retrieve the trait-R_{dark25} relationships across forest types. We found that our 'cross-site' spectral models were the most robust for R_{dark25} prediction (r^2=0.65, RMSE=0.17 μmol CO_2 m^{-2} s^{-1}) and performed better than the multivariate model based on leaf traits (R^2=0.30, RMSE=0.25 μmol CO_2 m^{-2} s^{-1}) (Figs. 4b&5). Meanwhile, the 'cross-site' spectral models captured the variations in all the other leaf traits including LMA (r^2=0.96, RMSE=6.78 g m^{-2}), leaf Mn (r^2=0.79, RMSE=0.03 g m^{-2}), Mg (r^2=0.77, RMSE=0.04 g m^{-2}), N (r^2=0.74,

RMSE=0.20 g m^{-2}), P (r^2=0.72, RMSE=0.02 g m^{-2}), Ca (r^2=0.71, RMSE=0.21 g m^{-2}), K (r^2=0.71, RMSE=0.18 g m^{-2}) and S (r^2=0.70, RMSE=0.03 g m^{-2}) concentrations across forest types (Fig. S8a-h). The linear relationships between spectrally derived traits and spectrally derived R_{dark25} were highly consistent with those obtained from field measurements, with commensurable r^2, slopes and intercepts for these two types of leaf trait relationships (Fig. S9a-h). In addition, we found that while the contributions of inter- and intraspecific variation to R_{dark25} variability were similar between the spectra-modelled and field-measured methods, the interspecific variation was slightly greater in the spectrally-modeled approach (Fig. 6a-d). These results verified that leaf reflectance spectroscopy provided an accurate alternative for inferring R_{dark25} and trait-R_{dark25} relationships across diverse forest types.

To further test the generalizability of spectra-R_{dark25} relationships, we cross-compared the spectra-R_{dark25} models under 'site-specific' and 'cross-site' scenarios. As shown in Fig. 5 *vs.* Fig. 7 and Table 1, the 'cross-site' model outperformed 'site-specific' models across different forest types (r^2=0.65, RMSE=0.17 μmol CO_2 m^{-2} s^{-1}) (Fig. 5), followed by the 'site-specific' XSBN model (r^2=0.56, RMSE=0.19 μmol CO_2 m^{-2} s^{-1}) (Fig. 7c), GT model (r^2=0.28, RMSE=0.25 μmol CO_2 m^{-2} s^{-1}) (Fig. 7b), and CB model (r^2=0.23, RMSE=0.35 μmol CO_2 m^{-2} s^{-1}) (Fig. 7a). Importantly, as the number of species or range of R_{dark25} included in the data of 'site-specific' model training subset decreased, the models exhibited worse performance and increased bias (as indicated by the RMSE and slopes) when applied to predict R_{dark25} for the sites not involved in the spectral modeling (Fig. 7). These results suggest that an accurate and transferable spectra-R_{dark25} model could be developed only when sufficient ranges of R_{dark25} variability and species diversity were encompassed in the PLSR modeling.

To untangle the underlying mechanism of the cross-site spectral–R_{dark25} model, we identified key band for prediction by analyzing the patterns in the PLSR variable importance in projection (VIP) metrics and coefficients (Fig. 8). Specifically, our 'cross-site' spectra-R_{dark25} model revealed the important bands as follows (VIP>1, Liu *et al*., 2023): 1) 400-427 nm, 519-575 nm,

and 694-700 nm in the visible band; 2) 700-800 nm in the red edge band; 3) 800-924 nm in near infrared band; and 4) short-wave infrared band of 1374-1428 nm, 1645-1672 nm, 1860-1887 nm, 2156-2221 nm, and 2253-2315 nm (Fig. 8a).

Discussion

Leaf R_{dark25}, an important, complex but difficult-to-measure eco-physiological trait, significantly contributes to the whole-plant net carbon exchange, and is an important physiological parameter in many TBMs to estimate ecosystem respiration and global carbon cycling (Atkin *et al*., 2015; Huntingford *et al*., 2017; Butler et al., 2021; Ren *et al*., 2023). However, a coherent understanding and efficient monitoring of fine-scale R_{dark25} variability across forest types remain elusive. Here we revealed the relationships of R_{dark25} with usual suspects leaf traits and leaf reflectance spectra across diverse forest types spanning large environmental gradients. We made two important findings. First, we found that leaf Mg, Ca and Mn concentrations were important in explaining R_{dark25}, but the relationships between R_{dark25} and other leaf traits were relatively weak (r^2<=0.13) and forest type-specific. Second, leaf reflectance spectroscopy could be used to create a single robust model of R_{dark25} predictions across forest types (r^2=0.65), with the transferability of the spectra-R_{dark25} model dependent on the trait range and spectral diversity in the trait training data. Taken together, our study expands on the key determinants of R_{dark25}, and highlights the substantial potential of reflectance spectroscopy in fast, reliable and high-throughput monitoring of plant eco-physiological traits and carbon cycling.

Variations in R_{dark25} and R_{dark25}:V_{cmax25} ratio across diverse forest types

Our results revealed substantial variation in leaf R_{dark25} and the R_{dark25}:V_{cmax25} ratios within and across forest types in China spanning large environmental gradients. The observations agree with previous field-based or global-scale synthesis studies regarding the latitudinal pattern of leaf respiratory and photosynthetic traits (Reich *et al*., 1998b; Wright *et al*., 2006; Atkin *et al*., 2015). While the large within-site variation may have weakened the effect of climate gradients

and makes R_{dark25}:V_{cmax25} lower in temperate forests than in tropical forests, which is different from previous studies (Atkin *et al*., 2015). This variation may have several possible explanations, including the thermal acclimation responses of respiratory metabolism, contrasting species survival strategies and nutrient availability, which all affect the cost of investments in the respiratory apparatus and the balances between respiratory and photosynthetic metabolism (Lambers, 1985; Reich *et al*., 1998a; Atkin & Tjoelker, 2003; Ren *et al*., 2023). As a result, despite the strong functional coupling between R_{dark25} and V_{cmax25} underpinned by chloroplast-mitochondrion interdependence, the proportionality of the two traits varies across species types and environmental conditions (Reich *et al*., 1998b; Atkin *et al*., 2015). However, despite the dynamic nature of both R_{dark25} and R_{dark25}:V_{cmax25} observed here and previously, a PFT-specific R_{dark25} value or constant R_{dark25}:V_{cmax25} ratio still remain widely used in TBMs to simulate plant respiration (Schwalm *et al.* 2010; Clark *et al*., 2011; Fan *et al*., 2021). Our results show that compared to what is in some TBMs, R_{dark25} at a given V_{cmax25} is higher in our forest types (R_{dark25}:V_{cmax25} ratio ranging from 0.019 to 0.026) than commonly assumed (0.015), which means the TBMs would underestimate R_{dark}. Therefore, we suggest incorporating more flexible parameterization schemes in TBMs to better capture the variation in large-scale terrestrial respiration, and model the associated carbon fluxes under the current and changing climate (Kyker-Snowman *et al*., 2022).

Biochemical traits reveal additional sources of leaf R_{dark25} variability

Leaf trait-R_{dark25} relationships are widely used to derive R_{dark25} from other morphological and biochemical traits, and formulate the empirical equations to facilitate the representation of R_{dark25} in TBMs (Atkin *et al*., 2015; Rowland *et al*., 2016). Among those traits, LMA, leaf N and P concentrations are often used, given their important roles in leaf construction costs, protein turnover, N assimilation, mitochondrial electron transport and glycolysis, which are functionally inter-dependent with leaf respiratory metabolism (Meir *et al*., 2001; Tjoelker *et al*., 2002; Fernie *et al*., 2004; Turnbull *et al*., 2005). Our results demonstrated weak ($r^2 \leq 0.06$) and forest type-specific relationships of R_{dark25} with these three traits (Fig. 3a-c), which are

consistent with previous studies that reported the moderate-to-weak trait-R_{dark25} relationships across different PFTs, growth environments and biogeographical regions (Wright *et al.*, 2006; Reich *et al*., 2008; Atkin *et al*., 2015; Wang *et al*., 2020a). These observed weak and dynamic trait-R_{dark25} relationships within and across sites might be attributed to the differences in nutrient allocation to metabolic versus structural components, distinct species compositions, and the interactions among leaf traits (Millar *et al*., 2011; Atkin *et al*., 2015; O'Leary *et al*., 2018; Rowland *et al*., 2018). Our study, together with previous findings, therefore suggest that there is no single universal scaling relationship accounting for R_{dark25} over large biogeographical extents. In other words, some prevailing relationships between traits and R_{dark25} observed at the global scale has limited predictability at fine-scale. This highlights the uncertainty of leveraging the conventional leaf trait relationships for characterizing cross-site R_{dark25} variability.

In addition to the aforementioned three leaf traits, we further analyzed multiple leaf morphological and biochemical traits as determinants of R_{dark25}, and found the best predictor of cross-site R_{dark25} variability was leaf Mg concentration, followed by leaf Ca, N, Mn, S and P concentrations, with minor roles of LMA and leaf K concentration (Figs. 3&4). Despite this order, together they control much of R_{dark25} variability. This study quantified the relationships between multiple leaf elemental concentrations and R_{dark25} over a large biogeographical scale, and highlights the important but previously unexpected roles of leaf Mg, Ca, Mn and S concentrations in explaining variability in R_{dark25}. Given the physiological functions of Mg, Ca, and S in mitochondrial activities (Millar *et al.*, 2011; Bhosale *et al.*, 2015; Rueda *et al.*, 2016; Chen *et al.*, 2018; Fratte *et al.*, 2021), this may be the main reason for their positive relationship with leaf dark respiratory flux across forest types. It is worth noting that Mg and Ca, as the two most important elements affecting R_{dark25}, also have strong covariation (Fig. S6), suggesting that there may be a pathway between them connected through respiratory metabolism. In contrast with Mg, Ca and S, Mn was negatively correlated with R_{dark25} (Fig. 3g), which has also been described in previous studies (Li *et al.*, 2010; Takagi *et al.*, 2021). The negative

503 correlation of Mn and Mg shows that there is also a competitive relationship between the
504 utilization of the two elements by leaves not only on cell scale but on a large scale (Fig. S6),
505 resulting in their opposite regulations on leaf respiratory metabolism (Bloom & Kameritsch,
506 2017; Bloom & Lancaster, 2018). The Mn-induced decrease in dark respiration may suggest
507 that the Mn concentrations observed in this study have reached a certain range of toxicity,
508 because excessive Mn inhibits NAD-malic enzyme activity (Takagi *et al*., 2021) or alter
509 stomatal and leaf anatomical development, causing stomatal dysfunction, and thus inhibit the
510 activities of both carbon anabolism and catabolism (Li *et al*., 2010). Collectively, all of the
511 examined eight leaf traits jointly contribute to 30% of cross-site R_{dark25} variability, which still
512 leaves a large proportion of unexplained R_{dark25} variance, which might be associated with many
513 other unconsidered factors, such as temperature acclimation, drought, leaf ontogeny,
514 phylogeny, and leaf metabolic traits and metabolic status (Atkin *et al*., 2009, 2011; Reich *et*
515 *al*., 2016; O'Leary *et al*., 2017; Yan *et al*., 2023). Further studies are thereby needed to reveal
516 the mechanisms underlying the R_{dark25} variability across forest types with the integration of
517 more relevant abiotic and biotic sources.
518
519 **Spectroscopy is an effective alternative for monitoring and understanding cross-site**
520 **R_{dark25} variability**
521 Our results showed that leaf reflectance spectroscopy outperformed traditionally-used leaf trait
522 relationships in predicting R_{dark25} across sites (r^2=0.65 vs. 0.30, RMSE=0.17 vs. 0.25 μmol CO_2
523 m^{-2} s^{-1}; Figs. 4a and 5). To the best of our knowledge, this is the first demonstration of R_{dark25}
524 prediction across forest types using hyperspectral spectra, although previous studies have also
525 shown the efficiency of spectral models in a limited number of species or vegetation types
526 (with relatively few species and limited size of the overall dataset) or of a single species, wheat
527 (Doughty *et al.*, 2011; Coast *et al.*, 2019; Lamour *et al.*, 2021). Our findings of the accurate
528 (r^2=0.70-0.96) cross-site spectral modeling of other eight traits also consolidated the recent
529 studies in which leaf reflectance spectroscopy could accurately infer important leaf
530 biochemical, morphological and physiological traits across different plant functional groups

and ecosystems (Ely *et al.*, 2019; Nakaji *et al.*, 2019; Kothari *et al.*, 2023). These results therefore reinforce that leaf reflectance spectroscopy offers a viable alternative for monitoring multiple trait dimensions across diverse plant species and growth environments, and can particularly enrich trait databases to fill in the key observational gaps in those difficult-to-measure physiological traits.

Given the likely lack of direct spectral absorption features by components in the respiratory systems, the spectra-R_{dark25} model may rely on the absorption features that are not causally associated with the target trait, but rather indirectly via other covarying traits such as pigments, leaf structure and water content driving the spectral changes ('constellation effects'; Chadwick and Asner, 2016; Nunes *et al*., 2017). The identified R_{dark25}-sensitive spectral bands are similar to the findings from a previous study on tropical forests (Lamour *et al.*, 2021) and are often shown to be sensitive to leaf biochemical traits (leaf Mg, Ca, N, Mn, S and P) (Kokaly *et al*., 2009; Osco *et al*., 2020; Liu *et al*., 2023; also see Fig. 8). The appearance of similar VIP peaks for leaf traits could be reflective of the shared functional roles. While leaf biochemical traits exhibit similar reflectance patterns to R_{dark25}, their weak explanatory power shown highlights the complexity of these relationships and their potential influence by additional factors. Meanwhile, these identified spectral bands are related to other leaf biochemical and physiological properties. The visible range has been connected with cell pigments; for example, chlorophyll absorbs red and blue light while reflecting green, which gives leaves their characteristic color and is closely linked to leaf nitrogen levels (Ustin *et al*., 2009; Wang *et al*., 2020b). The red-edge range is associate with chlorophyll, chlorophyll fluorescence and V_{cmax25} (Zarco-Tejada *et al*., 2000; Yan *et al*., 2021), while the detected NIR and SWIR bands are tightly associated with water content, lignin, cellulose, and the amount of starch or lipid, which are substrates for respiration (Kokaly *et al*., 2009; Lamour *et al*., 2024). These suggest that other unmeasured traits or processes might also participate in the indirect prediction of R_{dark25}, and spectroscopy may have potential for simultaneously monitoring a full suite of leave traits. However, when comparing observed and spectrally predicted trait relationships, we observed

559 that the r^2 values were generally higher for spectrally predicted relationships (Fig. S9), likely
560 due to the non-independence of the estimates, as both traits and R_{dark25} are derived from spectral
561 measurements. This may indicate that the spectra-modelled trait relationships tend to compress
562 the variation and reduce large residuals, suggesting potential biases in the strength of the
563 estimated trait covariance.
564
565 Another important finding was that the cross-site general spectra-R_{dark25} model can be built
566 only when leaf samples covering sufficient variability in both R_{dark25} and leaf reflectance
567 spectra are incorporated into the model development. This finding is supported by two aspects:
568 1) the spectra-R_{dark25} model under 'cross-site' scenario largely outperformed those under the
569 'site-specific' scenario (Figs. 5&7a-c); and, 2) the spectra-R_{dark25} model under the 'site-specific'
570 scenario showed much higher accuracy for its own forest site in contrast with the other two
571 sites not involved in the model development (Table 1). Previous studies have observed that
572 both leaf reflectance spectra and R_{dark25} change remarkably with ecosystems, plant functional
573 groups, climate conditions and leaf ages (Reich *et al*., 1998b; Atkin *et al*., 2015; Smith & Dukes,
574 2018; O'Leary *et al*., 2023). However, most of these drivers of R_{dark25} are still not sufficiently
575 captured in our study. Notably that most of the variation in spectrally predicted traits appears
576 to be interspecific rather than intraspecific (Fig. 6). This finding underscores the necessity of
577 considering trait variability at larger taxonomic scales when developing spectra-based models
578 (Kothari *et al*., 2023). Although site-specific models effectively capture variations driven by
579 the local environmental and biological factors of specific forest types (Lamour *et al*., 2021),
580 they lack the ecological heterogeneity necessary to generalize across greater biogeographical
581 gradients. In cross-site modeling, while some precision at individual sites may be sacrificed,
582 the model's adaptability across different biogeographic regions is significantly enhanced.
583 These results suggested that a more general and transferable spectra-R_{dark25} model would
584 require significantly broader and more diverse datasets, covering a wide range of leaf traits and
585 spectra across diverse plant functional types and ecosystems (Serbin *et al*., 2019; Burnett *et al.*,
586 2021; Ji *et al*., 2024). However, while this step is promising, we still have some distance from

being able to rely solely on spectroscopy to predict complex traits like R_{dark25} with high accuracy. Achieving this will likely involve trade-offs, such as accepting some reduction in site-specific precision in exchange for broader applicability. To effectively use spectroscopy at large scales, establishing a robust validation framework is also essential to ensure reliable predictions across diverse ecosystems.

Caveats and future directions

This work identifies two important next steps that need to be considered for future advances. First, our study collected leaf samples only from the top-canopy stratum of three typical forest sites at the peak of the growing season, which cover just a small fraction of Earth's vast plant diversity and omit many other important biomes, such as tundra, grasslands, shrublands and wetlands. Therefore, to test the robustness and generalizability of the mechanistic linkages of R_{dark25} to multiple leaf traits (particularly Mg, Ca, Mn and S) and leaf reflectance spectra, additional efforts would be needed to cover broader breadths of leaf trait and spectral variations (Kothari *et al*., 2023; Ji *et al*., 2024). Meanwhile, R_{dark25}, leaf traits and reflectance spectra vary remarkably throughout the vertical profiles within the canopy (Niinemets *et al*., 2015; Lamour *et al*., 2023), and across seasonal changes with different leaf developmental stages and environmental factors (Chen *et al*., 2022; Davidson *et al*., 2023a). Therefore, a comprehensive understanding and spectra-model evaluation of the R_{dark25} across more representative field sites, vertical structural gradients and full growing season are still imperative. The continued combination of traditional leaf gas exchange measurements and reflectance spectroscopy as part of global efforts are needed to further enable the development of generalized spectra-R_{dark25} model that can be applied in broad conditions. This can help incorporate a spectra-based data assimilation module into ecosystem models, and revolutionize the parameterization approach by directly integrating trait information rather than relying on predefined empirical relationships between traits (Fu *et al.*, 2020). Notably, currently a fully open database (Global Spectra Trait Initiative) for leaf-level physiological and spectral data is being assembled to

enable the continued development of spectra-trait models (https://github.com/plantphys/gsti/tree/main).

Second, given the sampling difficulties caused by canopy access have limited the measurement of R_{dark25} over large spatial extents, an alternative and rapid remote sensing method based on imaging spectroscopy technology is needed to monitor large-scale R_{dark25}. Canopy spectra can be collected using a range of platforms including unoccupied aerial systems (UAS; Yang *et al.* 2022), piloted airborne sensors and spaceborne satellites (Serbin & Townsend, 2020; Liu *et al.*, 2024), and it has been demonstrated to be effective in monitoring leaf traits associated with R_{dark25} (e.g., V_{cmax25}, leaf N, P concentrations, and LMA) (Liu *et al.*, 2023). Moreover, as the spectral variability of the canopy monitored by imaging spectroscopy mainly comes from the leaf spectrum (Asner, 1998), understanding the leaf-level spectra-R_{dark25} relationships is beneficial to the spectral modeling and potential vegetation indices developing of R_{dark25} at larger spatial scales (Serbin & Townsend, 2020). Therefore, future studies should explore R_{dark25} using various imaging spectroscopy platforms and try to extend leaf spectral models to canopy and ecosystem scales. This will require the development of appropriate hybrid modelling and validation approaches (Fu et al., 2020). During the upscaling process across different spatial resolutions, issues including the effects of canopy structure (Liu *et al.*, 2023) and environmental noisy (Asner, 1998; Ollinger, 2011; Cimoli *et al.*, 2024) need to be attention. As the community addresses challenges, spectroscopy will further contribute to explanation of more detailed scale-dependent mechanisms and monitoring of terrestrial plant respiration and carbon uptake capacities over large spatiotemporal extents (Serbin *et al.*, 2015; Jetz *et al.*, 2016; Yan *et al.*, 2021; Liu *et al.*, 2024). Our ultimate hope is that by combining field data with cutting-edge remote sensing technology, we will not only expand our understanding of knowledge of plant physiological traits, but also help us better diagnose the role and fate of terrestrial ecosystems under climate change.

Acknowledgements

This work was supported by Key Talent Project of the State Key Laboratory of Vegetation and Environmental Change (LVEC-2023rc01). OA is supported by an Australian Research Council Discovery Project grant (DP220101882). SPS is supported by the NASA Surface Biology and Geology Mission. AR was supported by the Next Generation Ecosystem Experiments - Tropics project funded by the US Department of Energy, Office of Science, Office of Biological and Environmental Research and by the U.S. Department of Energy Contract No. DE-AC02-05CH11231 to Lawrence Berkeley National Laboratory. Prof. D. Ellsworth from Western Sydney University is thanked for valuable comments on the manuscript. The authors would like to thank the Research Station of Changbai Mountain Forest Ecosystems, Zhejiang Qianjiangyuan Forest Biodiversity National Observation and Research Station, and National Forest Ecosystem Research Station at Xishuangbanna for canopy crane access assistance.

Competing interests

None.

Author contributions

ZY and FW planned and designed the research. FW, NY, TD, WX, GD, and JD performed experiments and conducted fieldwork. FW, and ZY analysed data with inputs from SL, JW, and HW. All authors contributed to interpreting the results. FW drafted the manuscript with constructive input from ZY, and all authors contributed to the manuscript editing.

Data availability statement

The data supporting the results of the manuscript can be accessed via the Plant Science Data Center, Chinese Academy of Sciences using the following link: XXXX.

667 **References**

668 **Akalusi ME, Meng FR, Bourque CP-A. 2021.** Photosynthetic parameters and stomatal
669 conductance in attached and detached balsam fir foliage. *Plant-Environment Interactions*
670 **2**(4), 206–215.
671 **Asner GP. 1998.** Biophysical and biochemical sources of variability in canopy reflectance.
672 *Remote sensing of Environment* **64**(3), 234–253.
673 **Asner GP, Knapp DE, Anderson CB, Martin RE, Vaughn N. 2016.** Large-scale climatic
674 and geophysical controls on the leaf economics spectrum. *Proceedings of the National*
675 *Academy of Sciences of the United States of America* **113**: E4043–E4051.
676 **Atkin OK, Tjoelker MG. 2003.** Thermal acclimation and the dynamic response of plant
677 respiration to temperature. *Trends in Plant Science* **8**: 343–351.
678 **Atkin OK, Scheurwater I, Pons TL. 2007.** Respiration as a percentage of daily
679 photosynthesis in whole plants is homeostatic at moderate, but not high, growth
680 temperatures. *New Phytologist* **174**: 367–380.
681 **Atkin OK, Macherel D. 2009.** The crucial role of plant mitochondria in orchestrating drought
682 tolerance. *Annals of Botany* **103**: 581–597.
683 **Atkin OK. 2011.** Introduction to a Virtual Special Issue on plant respiration in variable
684 environments. *New Phytologist* **191**: 1–4.
685 **Atkin OK, Bloomfield KJ, Reich PB, Tjoelker MG, Asner GP, Bonal D, Bönisch G,**
686 **Bradford MG, Cernusak LA, Cosio EG, *et al.* 2015.** Global variability in leaf
687 respiration in relation to climate, plant functional types and leaf traits. *New Phytologist*
688 **206**: 614–636.
689 **Atkin OK, Bahar NHA, Bloomfield KJ, Griffin KL, Heskel MA, Huntingford C, de la**
690 **Torre AM, Turnbull MH. 2017.** Leaf Respiration in Terrestrial Biosphere Models. Plant
691 Respiration: Metabolic Fluxes and Carbon Balance. G. Tcherkez. Netherlands, Springer-
692 Nature. **43**: 107–142.
693 **Balmer Y, Vensel WH, Tanaka CK, Hurkman WJ, Gelhaye E, Rouhier N, Jacquot JP,**
694 **Manieri W, Schürmann P, Droux M, *et al.* 2004.** Thioredoxin links redox to the

regulation of fundamental processes of plant mitochondria. *Proceedings of the National Academy of Sciences of the United States of America* **101**:2642–2647.

Bernacchi CJ, Singsaas EL, Pimentel C, Portis AR Jr, Long SP. 2001. Improved temperature response functions for models of Rubisco-limited photosynthesis: in vivo Rubisco enzyme kinetics. *Plant, Cell & Environment* **24**, 253–259.

Bernacchi CJ, Bagley JE, Serbin SP, Ruiz-Vera UM, Rosenthal DM, Van Loocke A. 2013. Modelling C3 photosynthesis from the chloroplast to the ecosystem. *Plant, Cell & Environment* **36**: 1641–1657.

Bhosale G, Sharpe JA, Sundier SY, Duchen MR. 2015. Calcium signaling as a mediator of cell energy demand and a trigger to cell death. *Annals of the New York Academy of Sciences* **1350**: 107–116.

Bloom AJ, Kameritsch P. 2017. Relative association of Rubisco with manganese and magnesium as a regulatory mechanism in plants. *Physiologia plantarum* **161**: 545–559.

Bloom AJ, Lancaster KM. 2018. Manganese binding to Rubisco could drive a photorespiratory pathway that increases the energy efficiency of photosynthesis. *Nature Plants* **4**: 414–422.

Burnett AC, Anderson J, Davidson KJ, Ely KS, Lamour J, Li Q, Morrison BD, Yang D, Rogers A, Serbin SP. 2021. A best-practice guide to predicting plant traits from leaf-level hyperspectral data using partial least squares regression. *Journal of Experimental Botany* **72**: 6175–6189.

Butler EE, Wythers KR, Flores-Moreno H, Chen M, Datta A, Ricciuto DM, Atkin OK, Kattge J, Thornton PE, Banerjee A, *et al.* 2021. Updated respiration routines alter spatio-temporal patterns of carbon cycling in a global land surface model. *Environmental Research Letters* **16**: 104015.

Cakmak BI, Yazici AM. 2010. Magnesium: a forgotten element in crop production. *Better Crops* **94**(2): 23–25.

Chadwick KD, Asner GP. 2018. Landscape evolution and nutrient rejuvenation reflected in Amazon forest canopy chemistry. *Ecology Letters* **21**(7): 978–988.

723 **Chavana-Bryant C, Malhi Y, Anastasiou A, Enquist BJ, Cosio EG, Keenan TF, Gerard**
724 **FF. 2019.** Leaf age effects on the spectral predictability of leaf traits in Amazonian canopy
725 trees. *Science of The Total Environment* **666**: 1301–1315.
726 **Chen ZC, Peng WT, Li J, Liao H. 2018.** Functional dissection and transport mechanism of
727 magnesium in plants. *Seminars in Cell & Developmental Biology* **74**: 142–152.
728 **Ciais P, Sabine C, Bala G, Bopp L, Brovkin V, Canadell J, Chhabra A, DeFries R,**
729 **Galloway J, Heimann M, *et al*. 2014.** Carbon and other biogeochemical cycles. Climate
730 change 2013: The physical science basis. Contribution of Working Group I to the Fifth
731 Assessment Report of the Intergovernmental Panel on Climate Change, 465–570.
732 **Cimoli E, Lucieer A, Malenovský Z, Woodgate W, Janoutová R, Turner D, Haynes R,**
733 **Phinn S. 2024.** Mapping functional diversity of canopy physiological traits using UAS
734 imaging spectroscopy. *Remote Sensing of Environment* **302**: 113958.
735 **Clark DB., Mercado LM, Sitch S, Jones CD, Gedney N, Best MJ, Pryor M, Rooney GG,**
736 **Essery RLH, Blyth E, *et al.* 2011.** The Joint UK Land Environment Simulator (JULES),
737 model description – Part 2: Carbon fluxes and vegetation dynamics. *Geoscientific Model*
738 *Development* **4**: 701–722.
739 **Coast O, Shah S, Ivakov A, Gaju O, Wilson PB, Posch BC, Bryant CJ, Negrini ACA,**
740 **Evan JR, Condon AG, *et al.* 2019.** Predicting dark respiration rates of wheat leaves from
741 hyperspectral reflectance. *Plant, Cell & Environment* 42: 2133–2150.
742 **Cui J, Davanture M, Zivy M, Lamade E, Tcherkez G. 2019.** Metabolic responses to
743 potassium availability and waterlogging reshape respiration and carbon use efficiency in
744 oil palm. *New Phytologist* **223**: 310–322.
745 **Curran PJ. 1989.** Remote sensing of foliar chemistry. *Remote Sensing of Environment* **30**:
746 271–278.
747 **Davidson KJ, Lamour J, McPherran A, Rogers A, Serbin, SP. 2023a.** Seasonal trends in
748 leaf-level photosynthetic capacity and water use efficiency in a North American Eastern
749 deciduous forest and their impact on canopy-scale gas exchange. *New Phytologist* **240**(1):
750 138–156.

751 **Davidson KJ, Lamour J, Rogers A, Ely KS, Li Q, McDowell NG, Pivovaroff AL, Wolfe**
752 **BT, Wright SJ, Zambrano A, *et al.* 2023b.** Short-term variation in leaf-level water use
753 efficiency in a tropical forest. *New Phytologist* **237**(6): 2069–2087.
754 **Dechant B, Cuntz M, Vohland M, Schulz E, Doktor D. 2017.** Estimation of photosynthesis
755 traits from leaf reflectance spectra: Correlation to nitrogen content as the dominant
756 mechanism. *Remote Sensing of Environment* **196**: 279–292.
757 **Doughty CE, Asner GP, Martin RE. 2011.** Predicting tropical plant physiology from leaf and
758 canopy spectroscopy. *Oecologia* **165**: 289–299.
759 **Elvidge CD. 1990.** Visible and near infrared reflectance characteristics of dry plant materials.
760 *International Journal of Remote Sensing* **11**: 1775–1795.
761 **Ely KS, Burnett AC, Lieberman-Cribbin W, Serbin SP, Rogers A. 2019.** Spectroscopy can
762 predict key leaf traits associated with source–sink balance and carbon–nitrogen status.
763 *Journal of experimental botany* **70**: 1789–1799.
764 **Fan Y, Asao S, Furbank RT, von Caemmerer S, Day DA, Tcherkez G, Sage TL, Sage RF,**
765 **Atkin OK.** 2021. The crucial roles of mitochondria in supporting C4 photosynthesis. *New*
766 *Phytologist* **233**: 1083–1096.
767 **Ferguson JN, Jithesh T, Lawson T, Kromdijk J. 2023.** Excised leaves show limited and
768 species-specific effects on photosynthetic parameters across crop functional types.
769 *Journal of Experimental Botany* **74**(21), 6662–6676
770 **Fernie, AR, Carrari F, Sweetlove LJ. 2004.** Respiratory metabolism: glycolysis, the TCA
771 cycle and mitochondrial electron transport. *Current Opinion in Plant Biology* **7**: 254–261.
772 **Filzmoser P, Liebmann B, Varmuza K. 2009.** Repeated double cross validation. *Journal of*
773 *Chemometrics* **23**: 160–171.
774 **Fratte MD, Pierce S, Zanzottera M, Cerabolini BEL. 2021.** The association of leaf sulfur
775 content with the leaf economics spectrum and plant adaptive strategies. *Functional Plant*
776 *Biology* **48**: 924–935.

Fu P, Meacham-Hensold K, Guan KY, Wu J, Bernacchi C. 2020. Estimating photosynthetic traits from reflectance spectra: A synthesis of spectral indices, numerical inversion, and partial least square regression. *Plant, Cell & Environment* **43**: 1241–1258.

Garcia A, Gaju O, Bowerman AF, Buck SA, Evans JR, Furbank RT, Gilliham M, Millar AH, Pogson BJ, Reynolds MP, *et al.* 2022. Enhancing crop yields through improvements in the efficiency of photosynthesis and respiration. *New Phytologist* **237**: 60–77.

Gelhaye E, Rouhier N, Gerard J, Jolivet Y, Gualberto J, Navrot N, Ohlsson P, Wingsle G, Hirasawa M, Knaffet DB, *et al.* 2004. A specific form of thioredoxin *h* occurs in plant mitochondria and regulates the alternative oxidase. *Proceedings of the National Academy of Sciences of the United States of America* **101**:14545–14550.

Guillén-Escribà C, Schneider FD, Schmid B, Tedder A, Morsdorf F, Furrer R, Hueni A, Niklaus PA, Schaepman ME. 2021. Remotely sensed between individual functional trait variation in a temperate forest. *Ecology and Evolution* **11**, 10834–10867.

Guo ZF, Yan ZB, Majcher BM, Lee CKF, Zhao YY, Song GQ, Wang B, Wang X, Deng Y, Michaletz ST, *et al.* 2022. Dynamic biotic controls of leaf thermoregulation across the diel timescale[J]. *Agricultural and Forest Meteorology* **315**: 108827.

Haynes RS, Lucieer A, Brodribb TJ, Tonet V, Cimoli E. 2024. Predicting key water stress indicators of *Eucalyptus viminalis* and *Callitris rhomboidea* using high-resolution visible to short-wave infrared spectroscopy. *Plant, Cell & Environment* https://doi.org/10.1111/pce.15083

He N, Liu C, Piao S, Sack L, Xu L, Luo Y, He J, Han X, Zhou G, Zhou X, *et al.* 2019. Ecosystem traits linking functional traits to macroecology. *Trends in Ecology and Evolution (Amst.)* **34**: 200–210.

Hu Z, Yu M, Suo F. 2005. The plant species diversity of the evergreen broad-leaved forest in Gutian Mountain National Nature Reserve. *Chinese Agricultural Science Bulletin (Chin Ver)* **21**(3): 134–137. (in Chinese)

Huntingford C, Atkin OK, Martinez-de la Torre A, Mercado LM, Heskel MA, Harper AB, Bloomfield KJ, O'Sullivan OS, Reich PB, Wythers KR. *et al.* 2017. Implications

of improved representations of plant respiration in a changing climate. *Nature Communications* **8**: 1602.

Jetz W, Cavender-Bares J, Pavlick R, Schimel D, Davis FW, Asner GP, Guralnick R, Kattge J, Latimer AM, Moorcroft P, *et al*. 2016. Monitoring plant functional diversity from space. *Nature Plants* **2**: 16024.

Ji FJ, Li F, Hao DL, Shiklomanov AN, Yang X, Townsend PA, Dashti H, Nakaji T, Kovach KR, Liu HR, *et al*. 2024. Unveiling the transferability of PLSR models for leaf trait estimation: lessons from a comprehensive analysis with a novel global dataset. *New Phytologist*. https://doi.org/10.1111/nph.19807

Kokaly RF, Asner GP, Ollinger SV, Martin ME, Wessman CA. 2009. Characterizing canopy biochemistry from imaging spectroscopy and its application to ecosystem studies. *Remote Sensing of Environment* **113**: S78–S91.

Kothari S, Beauchamp-Rioux R, Blanchard F, Crofts AL, Girard A, Guilbeault-Mayers X, Hacker PW, Pardo J, Schweiger AK, Demers-Thibeault S, *et al*. 2023. Predicting leaf traits across functional groups using reflectance spectroscopy. *New Phytologist* **238**(2): 549–566.

Kyker-Snowman E, Lombardozzi DL, Bonan GB, Cheng SJ, Dukes JS, Frey SD, Jacobs EM, McNellis R, Rady JM, Smith NG, *et al*. 2022. Increasing the spatial and temporal impact of ecological research: A roadmap for integrating a novel terrestrial process into an Earth system model. *Global Change Biology* **28**(2): 665–684.

Lambers H. 1985. Respiration in intact plants and tissues: its regulation and dependence on environmental factors, metabolism and invaded organisms. In: Douce R, Day DA, eds. *Encyclopedia of plant physiology, vol. 18*. New York, NY, USA: Springer-Verlag, 417–473.

Lambers H, Oliveira RS. 2008. *Plant physiological ecology (3rd ed.)*. New York: Springer, 115–172.

Lamour J, Davidson KJ, Ely KS, Anderson JA, Rogers A, Wu J, Serbin SP. 2021. Rapid estimation of photosynthetic leaf traits of tropical plants in diverse environmental conditions using reflectance spectroscopy. *PLoS ONE* **16**(10): e0258791.

Lamour J, Davidson KJ, Ely KS, Le Moguédec G, Anderson JA, Li QY, Calderón O, Koven CD, Wright SJ, Walker AP, *et al.* 2023. The effect of the vertical gradients of photosynthetic parameters on the CO_2 assimilation and transpiration of a Panamanian tropical forest. *New Phytologist* **238**(6): 2345–2362.

Li Q, C LS, Jiang HX, Tang N, Yang LT, Lin ZH, Li Y, Yang GH. 2010. Effects of manganese-excess on CO_2 assimilation, ribulose-1,5-bisphosphate carboxylase/oxygenase, carbohydrates and photosynthetic electron transport of leaves, and antioxidant systems of leaves and roots in *Citrus grandis* seedlings. *BMC Plant Biology* **10**: 42.

Liu SW, Yan ZB, Wang ZH, Serbin SP, Visser M, Zeng Y, Ryu Y, Su YJ, Guo ZF, Song GQ, *et al.* 2023. Mapping foliar photosynthetic capacity in sub-tropical and tropical forests with UAS-based imaging spectroscopy: Scaling from leaf to canopy. *Remote Sensing of Environment* **293**: 113612.

Liu SW, Wang ZH, Lin ZY, Zhao YY, Yan Z, Zhang K, Visser M, Townsend PA, Wu J. 2024. Spectra-phenology integration for high-resolution, accurate, and scalable mapping of foliar functional traits using time-series Sentinel-2 data. *Remote Sensing of Environment* **305**: 114082.

Long SP, Bernacchi CJ. 2003. Gas exchange measurements, what can they tell us about the underlying limitations to photosynthesis? Procedures and sources of error. *Journal of Experimental Botany* **54**(392): 2392–2401.

Maguire ME, Cowan JA. 2002. Magnesium chemistry and biochemistry. *Biometals* 15: 203–210.

Meacham-Hensold K, Montes CM, Wu J, Guan K, Fu P, Ainsworth EA, Pederson T, Moore CE, Brown KL, Raines C, *et al.* 2019. High-throughput field phenotyping using

hyperspectral reflectance and partial least squares regression (PLSR) reveals genetic modifications to photosynthetic capacity. *Remote sensing of environment* **231**: 111176.

Meir P, Grace J, Miranda AC. 2001. Leaf respiration in two tropical rainforests: constraints on physiology by phosphorus, nitrogen and temperature. *Functional Ecology* **15**: 378–387.

Millar AH, Whelan J, Soole KL and Day DA. 2011. Organization and regulation of mitochondrial respiration in plants. *Annu Rev Plant Biol* **62**: 79–104.

Nakaji T, Oguma H, Nakamura M, Kachina P, Asanok L, Marod D, Aiba M, Kurokawa H, Kosugi Y, Kassim, Abdul R, *et al.* 2019. Estimation of six leaf traits of East Asian Forest tree species by leaf spectroscopy and partial least square regression. *Remote Sensing of Environment* **233**, 111381.

Niinemets Ü, Keenan TF, Hallik L. 2015. A worldwide analysis of within-canopy variations in leaf structural, chemical and physiological traits across plant functional types. *New Phytologist* **205**(3): 973–993.

Ning Y, Chen S, Qian H, Ren H, Bebber D, Chen J. 2013. Diurnal and seasonal patterns of soil respiration in subtropical evergreen broad-leaved forests with different degrees of human disturbance in Gutianshan, Zhejiang Province. *Chinese Science Bulletin (Chin Ver)* **58**: 3839–3848. (in Chinese)

Nunes MH, Davey MP, Coomes DA. 2017. On the challenges of using field spectroscopy to measure the impact of soil type on leaf traits. *Biogeosciences* **14**(13), 3371–3385.

Okamoto S. 1967. Effects of potassium nutrition on the glycolysis and the krebs cycle in taro plants. *Soil Science and Plant Nutrition* **13**: 143–150.

Okamoto S. 1968. The respiration in the roots of broad bean and barley under a moderate potassium deficiency. *Soil Science and Plant Nutrition* **14**: 175–182.

O'Leary BM, Lee CP, Atkin OK, Cheng R, Brown TB, Millar AH. 2017. Variation in leaf respiration rates at night correlates with carbohydrate and amino acid supply. *Plant Physiology* **174**: 2261–2273.

O'Leary BM, Asao S, Millar AH, Atkin OK. 2018. Core principles which explain variation in respiration across biological scales. *New Phytologist* **222**: 670–686.

O'Leary BM, Scafaro AP, York LM. 2023. High-throughput, dynamic, multi-dimensional: an expanding repertoire of plant respiration measurements. *Plant Physiology* **191**(4), 2070–2083.

Ollinger SV, Smith ML. 2005. Net primary production and canopy nitrogen in a temperate forest landscape: an analysis using imaging spectroscopy, modeling and field data. *Ecosystems* **8**: 760–778.

Ollinger SV. 2011. Sources of variability in canopy reflectance and the convergent properties of plants. *New Phytologist* **189**(2): 375–394.

Osco LP, Ramos APM, Faita Pinheiro MM, Moriya ÉAS, Imai NN, Estrabis N, Ianczyk F, Araújo FFd, Liesenberg V, Jorge LAdC, *et al.* 2020. A Machine Learning Framework to Predict Nutrient Content in Valencia-Orange Leaf Hyperspectral Measurements. *Remote Sensing* **12**(6): 906.

Pedregosa F, Varoquaux G, Gramfort A, Michel V, Thirion B, Grisel O, Blondel M, Prettenhofer P, Weiss R, Dubourg V, *et al.* 2011. Scikit-learn: Machine learning in Python. *Journal of Machine Learning Research* **12**, 2825–2830.

R Core Team. 2013. R: a language and environment for statistical computing. Vienna, Austria: R Foundation for Statistical Computing.

Reich PB, Walters MB, Ellsworth DS, Vose JM, Volin JC, Gresham C, Bowman WD. 1998a. Relationships of leaf dark respiration to leaf nitrogen, specific leaf area and leaf life-span: a test across biomes and functional groups. *Oecologia* **114**: 471–482.

Reich PB, Walters MB, Tjoelker MG, Vanderklein D, Buschena C. 1998b. Photosynthesis and respiration rates depend on leaf and root morphology and nitrogen concentration in nine boreal tree species differing in relative growth rate. *Functional Ecology* **12**: 395–405.

Reich PB, Tjoelker MG, Pregitzer KS, Wright IJ, Oleksyn J, Machado JL. 2008. Scaling of respiration to nitrogen in leaves, stems and roots of higher land plants. *Ecology Letters* **11**: 793–801.

Reich PB, Sendall K, Stefanski A, Wei X, Rich RL, Montgomery RA. 2016. Boreal and temperate trees show strong acclimation of respiration to warming. *Nature* **531**, 633–636.

Ren YH, Wang H, Harrison SP, Prentice IC, Atkin OK, Smith NG, Mengoli G, Stefanski A, Reich PB, *et al.* 2023. Reduced global plant respiration due to the acclimation of leaf dark respiration coupled with photosynthesis. *New Phytologist* **241**: 578–591.

Rogers A, Serbin SP, Ely KS, Sloan VL, Wullschleger SD. 2017. Terrestrial biosphere models underestimate photosynthetic capacity and CO_2 assimilation in the Arctic. *New Phytologist* **216**: 1090–1103.

Rowland L, Zaragoza‐Castells J, Bloomfield KJ, Turnbull MH, Bonal D, Burban B, Salinas N, Cosio E, Metcalfe DJ, Ford A, *et al.* 2016. Scaling leaf respiration with nitrogen and phosphorus in tropical forests across two continents. *New Phytologist* **214**(3): 1064–1077.

Rowland L, da Costa ACL, Oliveira AAR, Oliveira RS, Bittencourt PL, Costa PB, Giles AL, Sosa AI, Coughlin I, Godlee JL, *et al.* 2018. Drought stress and tree size determine stem CO_2 efflux in a tropical forest. *New Phytologist* **218**(4): 1393–1405.

Rueda CB, Llorente-Folch I, Traba J, Amigo I, Gonzalez-Sanchez P, Contreras L, Juaristi I, Martinez-Valero P, Pardo B, del Arco A, *et al.* 2016. Glutamate excitotoxicity and Ca^{2+}-regulation of respiration: Role of the Ca^{2+} activated mitochondrial transporters (CaMCs). *Biochimica et Biophysica Acta (BBA) - Bioenergetics* **1857**: 1158–1166.

Satrústegui J, Pardo B, del Arco A. 2007. Mitochondrial transporters as novel targets for intracellular calcium signaling. *Physiological Reviews* **87**: 29-67.

Schwalm CR, Williams CA, Schaefer K, Anderson R, Arain MA, Baker I, Barr A, Black TA, Chen GS, Chen JM, *et al.* 2010. A model-data intercomparison of CO_2 exchange across North America: results from the North American Carbon Program site synthesis. *Journal of Geophysical Research: Biogeosciences* **115**: G00H05.

Serbin SP, Singh A, McNeil BE, Kingdon CC, Townsend PA. 2014. Spectroscopic determination of leaf morphological and biochemical traits for northern temperate and boreal tree species. *Ecological Applications* **24**: 1651–1669.

941 **Serbin SP, Singh A, Desai AR, SG Dubois, Jablonski AD, CC Kingdon, EL Kruger, PA**
942 **Townsend. 2015.** Remotely estimating photosynthetic capacity, and its response to
943 temperature, in vegetation canopies using imaging spectroscopy. *Remote Sensing of*
944 *Environment* **167**: 78–87.
945 **Serbin SP, Wu J, Ely KS, Kruger EL, Townsend PA, Meng R, Wolfe BT, Chlus A, Wang**
946 **ZH, Rogers A. 2019.** From the Arctic to the tropics: multibiome prediction of leaf mass
947 per area using leaf reflectance. *New Phytologist* **224**:1557–1568.
948 **Serbin SP, Townsend PA. 2020.** Scaling functional traits from leaves to canopies//Cavender-
949 Bares J, Gamon JA, Townsend PA. *Remote Sensing of Plant Biodiversity*. Springer, Cham,
950 Switzerland, 43–82.
951 **Shapiro JB, Griffin KL, Lewis JD, Tissue DT. 2004.** Response of *Xanthium strumarium* leaf
952 respiration in the light to elevated CO_2 concentration, nitrogen availability and
953 temperature. *New Phytologist* **162**: 377-386.
954 **Shen T, Corlett RT, Song L, Ma WZ, Guo XL, Song Y, Wu Y. 2018.** Vertical gradient in
955 bryophyte diversity and species composition in tropical and subtropical forests in Yunnan,
956 SW China. *Journal of Vegetation Science* **29**: 1075–1087.
957 **Smith NG, Dukes JS. 2018.** Drivers of leaf carbon exchange capacity across biomes at the
958 continental scale. *Ecology* **99**: 1610–1620.
959 **Takagi D, Ishiyama K, Suganami M, Ushijima T, Fujii T, Tazoe Y, *et al.* 2021.** Manganese
960 toxicity disrupts indole acetic acid homeostasis and suppresses the CO_2 assimilation
961 reaction in rice leaves. *Scientific Reports* **11**: 20922.
962 **Tcherkez G, Abadie C, Dourmap C, Lalande J, Limami AM. 2024.** Leaf day respiration:
963 More than just catabolic CO_2 production in the light. *Plant, Cell & Environment*, 1–9.
964 **Turnbull MH, Tissue DT, Griffin KL, Richardson SJ, Peltzer DA, Whitehead D. 2005.**
965 Respiration characteristics in temperate rainforest tree species differ along a long-term
966 soil-development chronosequence. *Oecologia* **143**: 271–279.

967 **Ustin SL, Gitelson AA, Jacquemoud S, Schaepman M, Asner GP, Gamon JA, Zarco-**
968 **Tejada P. 2009.** Retrieval of foliar information about plant pigment systems from high
969 resolution spectroscopy. *Remote Sensing of Environment* **113**: S67–S77.
970 **Verryckt LT, Van Langenhove L, Ciais P, Courtois EA, Vicca S, Peñuelas J, Stahl C,**
971 **Coste S, Ellsworth DS, Posada JM, *et al.* 2020.** Coping with branch excision when
972 measuring leaf net photosynthetic rates in a lowland tropical forest. *Biotropica.* 52: 608–
973 615.
974 **Von Caemmerer S. 2013.** Steady-state models of photosynthesis: steady-state models of
975 photosynthesis. *Plant, Cell & Environment* **36**, 1617–1630.
976 **Wang H, Atkin OK, Keenan TF, Smith NG, Wright IJ, Bloomfield KJ, Kattge J, Reich**
977 **PB, Prentice IC. 2020a.** Acclimation of leaf respiration consistent with optimal
978 photosynthetic capacity. *Global Change Biology* **26**: 2573–2583.
979 **Wang S, Guan K, Wang ZH, Ainsworth EA, Zheng T, Townsend PA, Li KY, Moller C,**
980 **Wu GH, Jiang CY. 2020b.** Unique contributions of chlorophyll and nitrogen to predict
981 crop photosynthetic capacity from leaf spectroscopy. *Journal of Experimental Botany* **72**:
982 341–354.
983 **Wang X, Wang CZ, Wu J, Miao GF, Chen M, Chen SL, Wang SH, Guo ZF, Wang ZH,**
984 **Wang B, *et al.* 2021.** Intermediate Aerosol Loading Enhances Photosynthetic Activity of
985 Croplands. *Geophysical Research Letters* **48**(7), e2020GL091893.
986 **Wold S, Sjöström M, Eriksson L. 2001.** PLS-regression: a basic tool of chemometrics.
987 *Chemometrics Intelligent Laboratory Systems* **58**, 109–130.
988 **Wright IJ, Reich PB, Atkin OK, Lusk CH, Tjoelker MG, Westoby M. 2006.** Irradiance,
989 temperature and rainfall influence leaf dark respiration in woody plants: evidence from
990 comparisons across 20 sites. *New Phytologist* **169**: 309–319.
991 **Wu J, Chavana‐Bryant C, Prohaska N, Serbin SP, Guan KY, Albert LP, Yang X, van**
992 **Leeuwen WJD, Garnello AJ, Martins G, *et al.* 2016.** Convergence in relationships
993 between leaf traits, spectra and age across diverse canopy environments and two
994 contrasting tropical forests. *New Phytologist* 214: 1033-1048.

Wu J, Rogers A, Albert LP, Ely K, Prohaska N, Wolfe BT, Oliveira Jr RC, Saleska SR, Serbin SP. 2019. Leaf reflectance spectroscopy captures variation in carboxylation capacity across species, canopy environment and leaf age in lowland moist tropical forests. *New Phytologist* **224**: 663–674.

Yan ZB, Guo ZF, Serbin SP, Song GQ, Zhao YY, Chen Y, Wu SB, Wang J, Wang X, Li J, *et al.* 2021. Spectroscopy outperforms leaf trait relationships for predicting photosynthetic capacity across different forest types. *New Phytologist* **232**, 134–147.

Yan ZB, Sardans J, Peñuelas J, Detto M, Smith NG, Wang H, Guo LL, Hughes AC, Guo ZF, Lee CKF, *et al.* 2023. Global patterns and drivers of leaf photosynthetic capacity: the relative importance of environmental factors and evolutionary history. *Global Ecology and Biogeography* **32**: 668–682.

Yang DD, Morrison BD, Davidson KJ, Lamour J, Li Q, Nelson PR, Hantson W, Hayes DJ, Swetnam TL, McMahon A, *et al.* 2022. Remote sensing from unoccupied aerial systems: Opportunities to enhance Arctic plant ecology in a changing climate. *Journal of Ecology* **110**: 2812–2835.

Zarco-Tejada PJ, Miller JR, Mohammed GH, Noland TL. 2000. Chlorophyll fluorescence effects on vegetation apparent reflectance: I. Leaf-level measurements and model simulation. *Remote Sensing of Environment* **74**: 582–595.

Supporting information

The following Supporting Information is available for this article:

Fig. S1 Comparison of the leaf spectral reflectance from leaves on the tree and excised branch.

Fig. S2 Cross-comparison of the leaf R_{dark25} derived using the temperature response functions in Atkin *et al.* (2015) and Davidson *et al.* (2022).

Fig. S3 Schematic illustration of the repeated double cross-validation (rdCV) method for partial least squares regression (PLSR).

Fig. S4 The selection criterion for the optimal number of latent components in the spectral model of leaf traits under the cross-site scenario.

Fig. S5 Histogram distribution of the coefficient of determination (R^2) for the PLSR spectral models over the 200 permutations under the cross-site scenario.

Fig. S6 Exploring the variabilities of leaf morphological and biochemical traits within and across forest sites.

Fig. S7 Pearson correlation analysis of leaf biochemical traits across the three forest sites.

Fig. S8 Accuracy assessment for the cross-site spectral models of leaf morphological and biochemical traits.

Fig. S9 Cross-comparisons between the observed (blue color) and spectra-modelled (red color) trait-R_{dark25} relationships across the three forest sites

Table S1 Soil information for the three forest sites in China.

Table S2 Summary of species, leaf traits and sample size of representative canopy trees across the three forest sites in China.

Table S3 Statistical summary of the relationships between R_{dark25} and the eight leaf morphological and biochemical traits across the three forest sites.

Method S1 Protocol of A-C_i curves measurement.

Method S2 Protocol of the measurements of morphological and biochemical traits, including LMA, leaf N, P, K, Ca, Mg, Mn and S concentrations.

Method S3 Protocol of PLSR modeling with rdCV.

Fig. 1 The location and basic information of the three typical forest sites in China. The three forest sites span a large latitudinal gradient, including a temperate forest in Mountain Changbai (CB), a subtropical forest in Mountain Gutian (GT), and a tropical rainforest in Xishuangbanna (XSBN). All the three forest sites have tower crane facilities enabling to access to the sunlit canopy leaves. The background shows a map of the 1:1,000,000 scale vegetation distribution of China provided by "Environmental & Ecological Science Data Center for West China, National Natural Science Foundation of China" (http://westdc.westgis.ac.cn). MAT, mean annual temperature; MAP, mean annual precipitation.

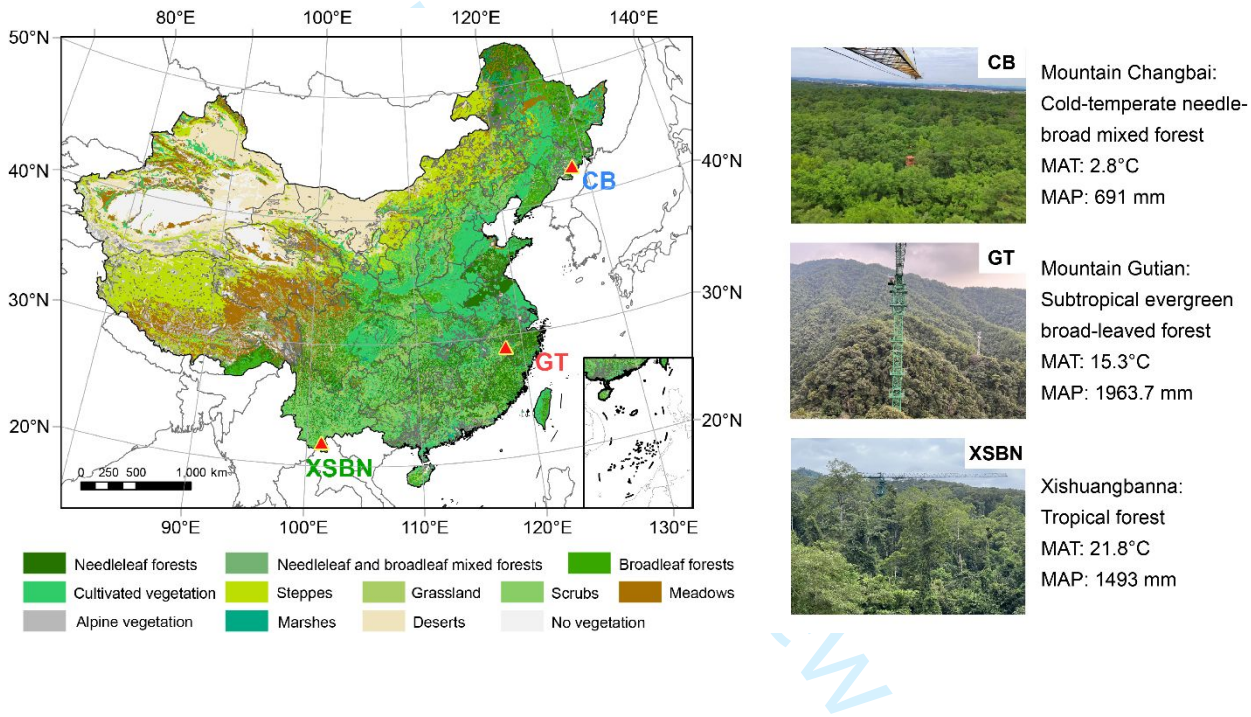

Fig. 2 The variability of R_{dark25} and its relationship with V_{cmax25} within and across forest sites. (a): The differences in R_{dark25} among diverse forest sites. (b): The differences in the ratio of R_{dark25} to V_{cmax25} (R_{dark25}:V_{cmax25}) among diverse forest sites. (c): R_{dark25}-V_{cmax25} relationships within and across forest sites. These values are gas-exchange measurements. One-way ANOVA with the least significant difference post-hoc test was used for the comparisons among the three forest sites. Different lower-case letters adjoining the violin plots indicate the significant difference (P<0.05) among different groups. The fitted lines were determined by ordinary least-squares regressions, showing significantly different slopes among the CB, GT, and XSBN sites, which represent temperate, subtropical, and tropical forests in China, respectively. The black line represents regression fit for all sites. r^2 is the coefficient of determination and the relationships are all significant (P<0.05).

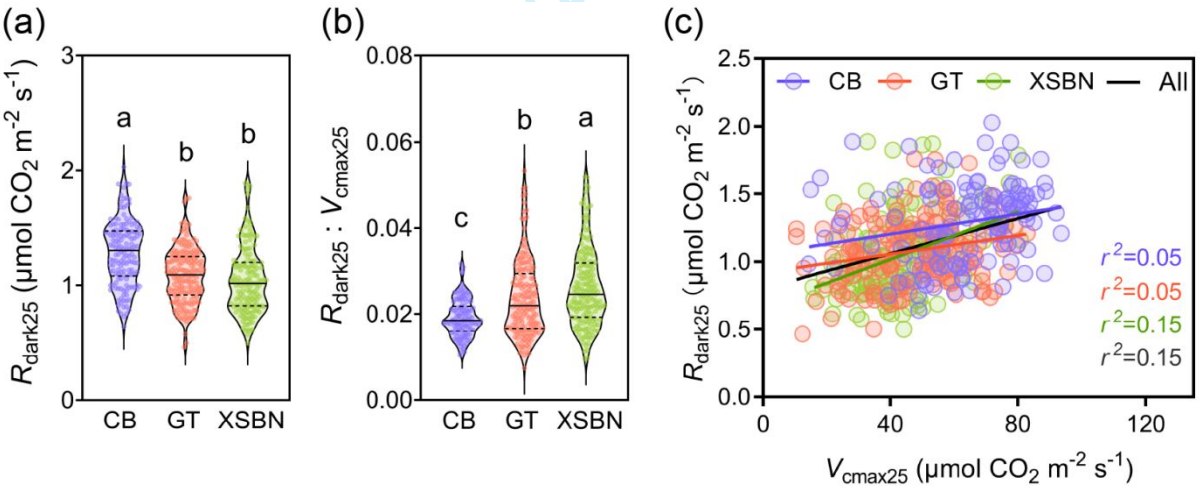

Fig. 3 The trait-R_{dark25} relationships within and across forest sites. (a-h): Pairwise relationships between R_{dark25} and eight leaf traits (i.e. LMA, and leaf N, P, K, Ca, Mg, Mn, and S concentration). The fitted lines are determined by the ordinary least squares regression, with colored lines representing regression fits for specific sites and black lines representing regression fit for all sites. r^2 is the coefficient of determination. All metrics and lines shown are statistically significant ($P < 0.05$).

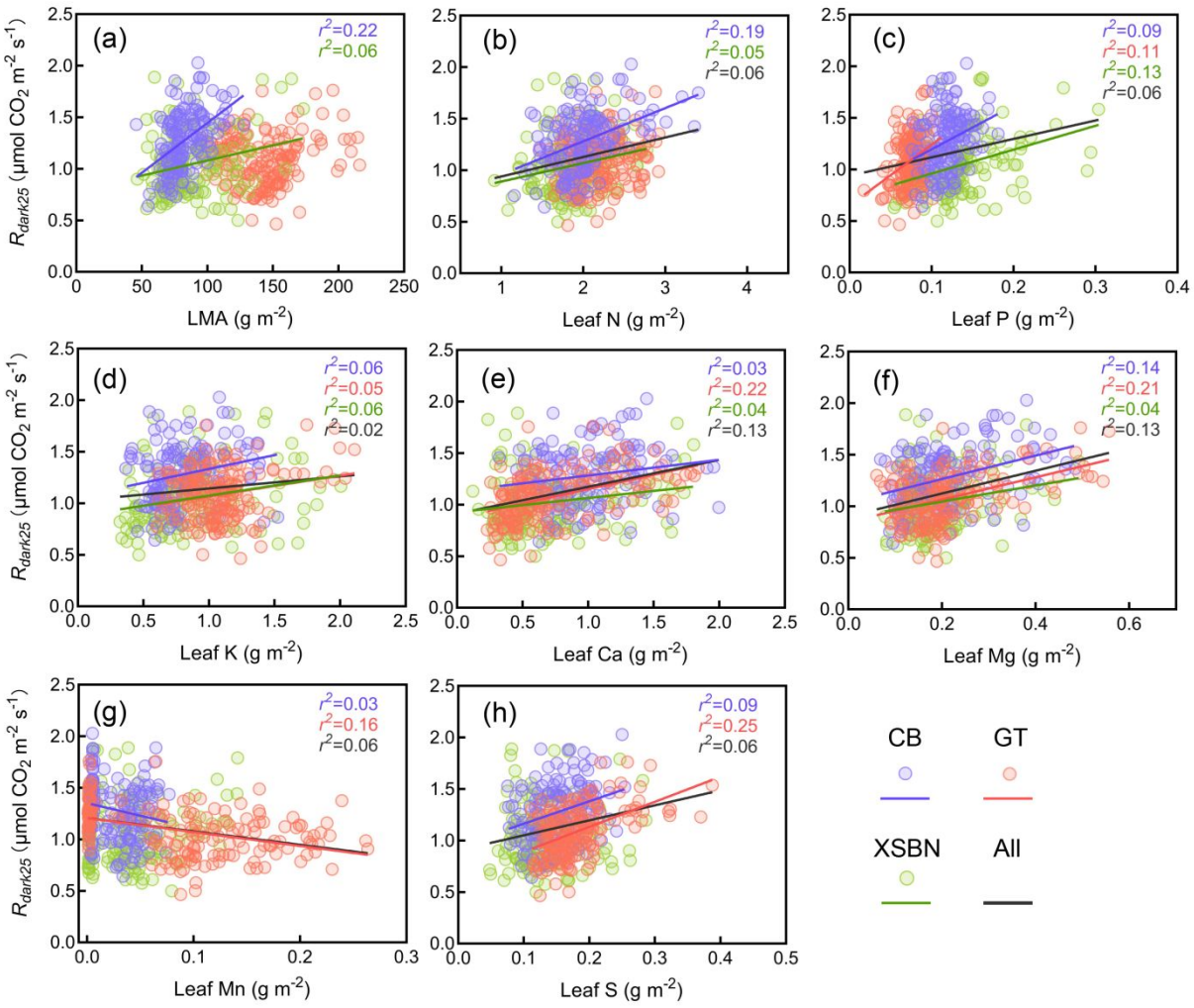

Fig. 4 The performance of multiple linear models for predicting R_{dark25} using all the other eight easy-to-measure leaf traits as predictor variables, and the relative importance of these predictor variables. (a): The relative importance of these traits on R_{dark25} prediction across forest sites, derived from their proportions of the explanation of the variance (r^2) indicated by the number adjoining the bars. (b): The performance of site-specific and cross-site model using multiple leaf traits (i.e. LMA, leaf N, P, Ca, Mg, Mn, and S concentrations) for predicting leaf R_{dark25}. The colored circles in the figure represent site-specific predictions (with Mountain CB in purple, GT in red, and XSBN in green), the grey circles represent the predictions of the cross-site linear mixed-effects model using site as random effects, and black line is the ordinary least squares fit of the cross-site model.

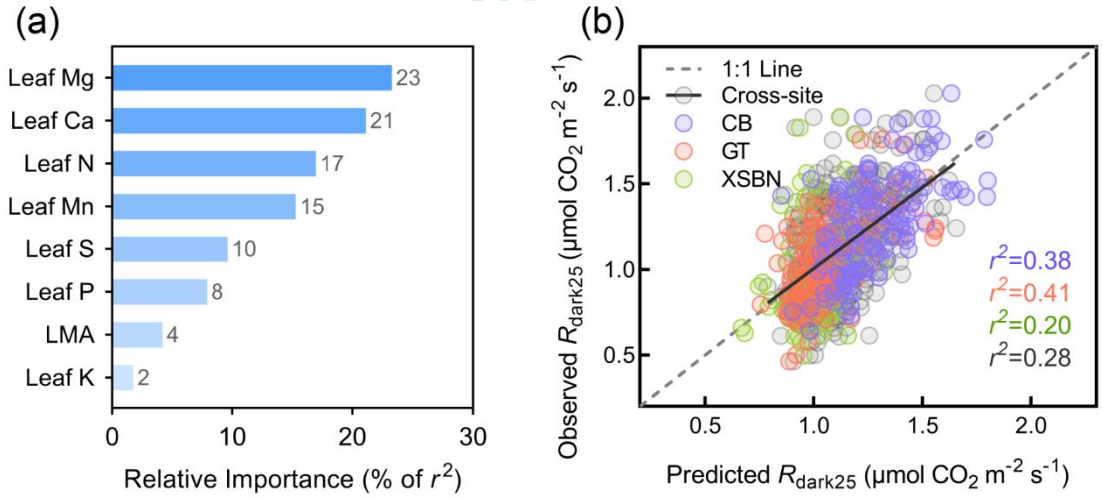

Fig. 5 Accuracy assessment for the cross-site spectra-R_{dark25} relationship. The cross-site model used the whole data set of leaf R_{dark25} and reflectance spectra from the three forest sites, and was trained and evaluated using the repeated double cross-validation method. The black line is the ordinary least-squares fit; the grey line indicates the 1:1 line. The colored points represent the predictions of the cross-site PLSR model for each forest site (with CB in purple, GT in red, and XSBN in green). *n*, sample size; r^2, the coefficient of determination; RMSE, the root mean square of error.

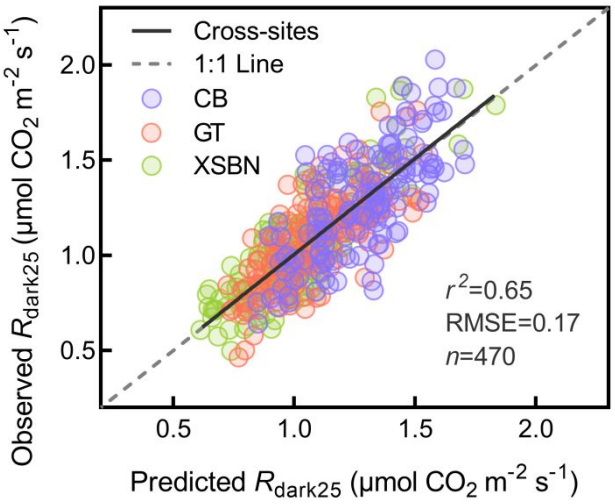

Fig. 6 Variance partitioning of leaf R_{dark25} and leaf morphological (i.e. LMA) and biochemical (i.e. leaf N, P, K, Ca, Mg, Mn and S concentrations) traits within (a-c) and across forest sites (d). The forest sites include the temperate forest in CB, the subtropical forest in GT, and the tropical forest in XSBN in China. The total variability for each trait was partitioned into intraspecific and interspecific components. The grey bars denote the variance partitioning from field-observed leaf traits, while the colored bars indicate the variance partitioning results from leaf traits predicted from the cross-site spectra-trait models.

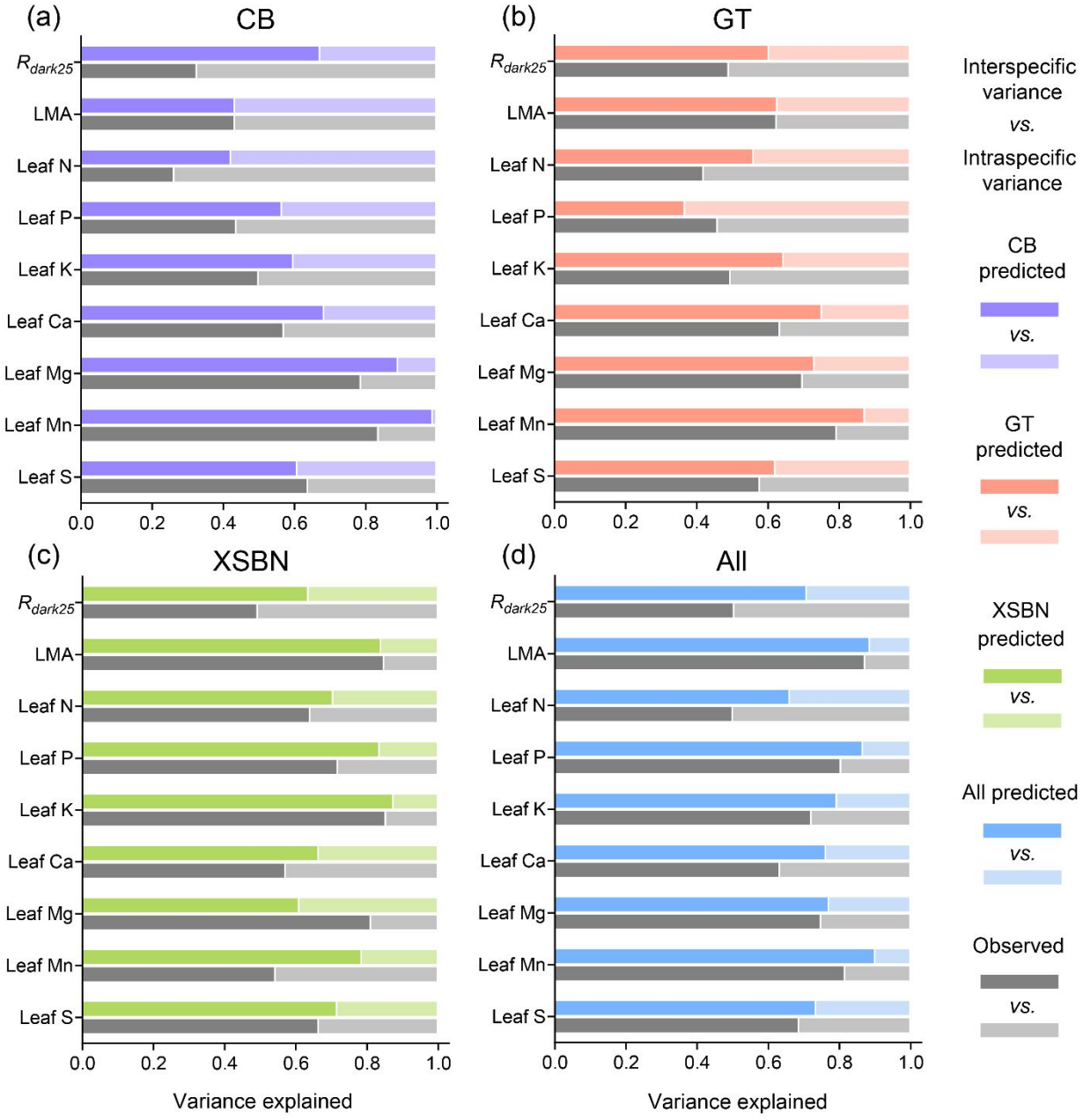

Fig. 7 Accuracy assessment for the spectra-R_{dark25} relationship under site-specific modeling scenarios. (a): CB model; (b): GT model; and (c): XSBN model. The site-specific models used specific data sets of leaf R_{dark25} and reflectance spectra within each of the three forest sites, was trained and evaluated using repeated double cross-validation method, and then was applied to the other two independent sites. The colored points and lines represent the predictions of the PLSR model and ordinary least squares fit for each forest site (with CB in purple, GT in Red, and XSBN in green). The number of species in CB model, GT model, and XSBN model are 10, 16, and 33, respectively.

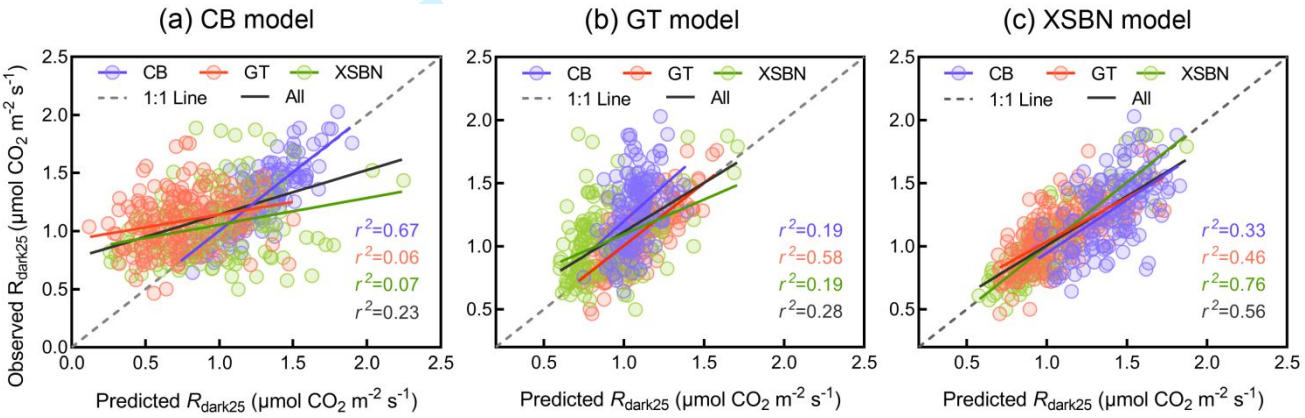

Fig. 8 Assessing the contributions of reflectance bands to the spectral models of leaf R_{dark25}, and the important R_{dark25} predictors (i.e. leaf Mg, Ca, N, Mn, S and P concentrations following the order of relative importance in predicting R_{dark25}) and LMA under the 'cross-site' scenario. The left panels (a-h) present the PLSR variable importance in projection (VIP), and the right panels (i-p) present the PLSR regression coefficients. The mean values and 95% confidence interval of the PLSR VIP spectrum and regression coefficients were indicated by central-colored lines and shaded regions, respectively. On the left panel, , the spectral regions with VIP $\geqslant$ 1 are those important for the spectral modeling of R_{dark25} and the important predictors (Lamour *et al.*, 2021; Liu *et al.*, 2023). The corresponding important spectral bands for R_{dark25} predictions are identified by the shaded grey regions across all subpanels. VIR, visible range (450–700 nm); RE, red-edge range (700–800 nm); NIR, near-infrared range (800–1300 nm); SWIR, shortwave infrared range (1300–2500 nm).

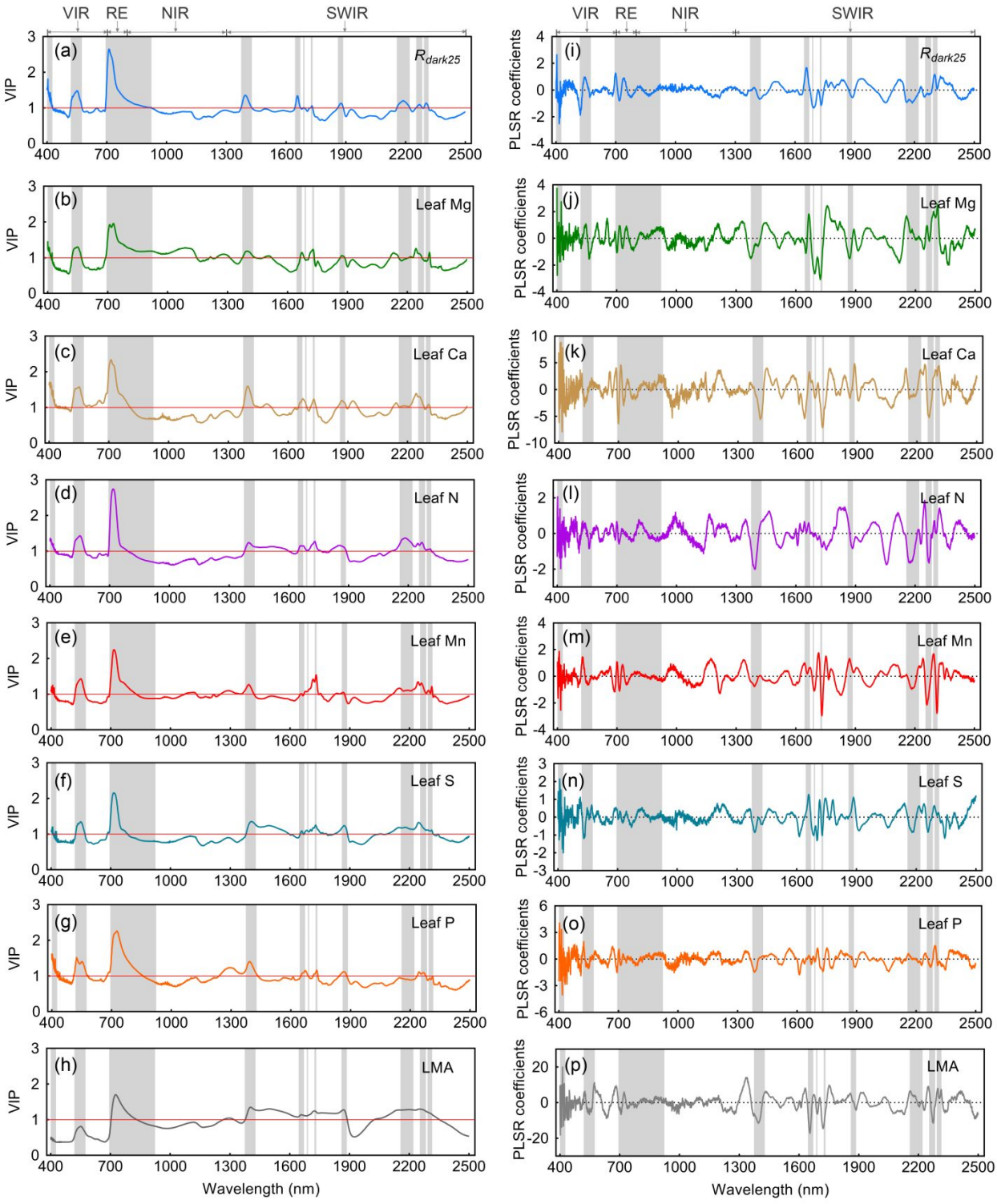
VIR
RE
NIR
SWIR
(a)
R_{dark25}
(b)
Leaf Mg
(c)
Leaf Ca
(d)
Leaf N
(e)
Leaf Mn
(f)
Leaf S
(g)
Leaf P
(h)
LMA
VIP
(i)
(j)
(k)
(l)
(m)
(n)
(o)
(p)
PLSR coefficients
Wavelength (nm)

1120

Table 1 Performance of the two types of spectra-R_{dark25} models: 'site-specific model' (trained and evaluated using the data from the single forest site respectively, and then applied to the other two independent sites), and 'cross-site model' (trained and evaluated using the data from all the three forest sites). The repeated double cross-validation method was used for training and evaluating all the models. The three diverse forest sites span large latitudinal gradients, including the temperate forest in CB, the subtropical forest in GT, and the tropical forest in XSBN.

		R_{dark25} (μmol CO_2 m^{-2} s^{-1})		
Scenarios	Site	*n*	r^2	RMSE
CB model	CB	146	0.67	0.16
	GT	173	0.06	0.46
	XSBN	151	0.07	0.35
	All	470	0.23	0.35
GT model	CB	146	0.19	0.31
	GT	173	0.58	0.15
	XSBN	151	0.19	0.28
	All	470	0.28	0.25
XSBN model	CB	146	0.33	0.25
	GT	173	0.46	0.18
	XSBN	151	0.76	0.13
	All	470	0.56	0.19
Cross-site model	CB	146	0.51	0.20
	GT	173	0.57	0.16
	XSBN	151	0.71	0.16
	All	470	0.65	0.17

Note: R_{dark25}, leaf dark respiration standardized to 25°C; *n*, sample size; r^2, the coefficient of determination; RMSE, the root mean square of error.

1121